Landscape and Urban Planning 165 (2017) 142–161

Contents lists available at ScienceDirect

Landscape and Urban Planning

journal homepage: www.elsevier.com/locate/landurbplan

Research paper

Assessing the impact of changes in surface cover, human behaviour and climate on energy partitioning across Greater London

H.C. Ward*, C.S.B. Grimmond*

Department of Meteorology, University of Reading, Reading, UK

ARTICLE INFO

Keywords:
City planning
Energy partitioning
Population growth
SUEWS model
Surface energy balance

ABSTRACT

Climate-sensitive urban design is an increasingly important consideration for city planners and policy makers. This study demonstrates the use of a biophysical model to assess the response of urban climate to various changes, including population growth, reduced energy use, urban development and urban greening initiatives. Model inputs are intentionally derived using only publicly available information and assumptions involved in collating the data are discussed. Results are summarised in terms of the energy partitioning which captures changes in meteorology, surface characteristics and human behaviour. The model has been recently evaluated for the region, and those findings are drawn upon here to discuss the model's capabilities and limitations. Model simulations demonstrate how both intentional and inadvertent changes to the urban landscape can alter the urban climate. For example, the impact of population growth depends on where, and how, people are housed, and recent changes in garden composition have reduced evaporation. This study has been designed so that model output could be combined with socio-economic data in future, enabling both risk and vulnerability to be considered together.

1. Introduction

Growth in urban populations puts increasing pressure on city planners, policy makers and society to develop in a sustainable and resilient manner. Cities must have the capacity to mitigate the impacts of extreme weather in order to minimise damage to human health, the environment and the economy. Urban climate-related risks include, but are not limited to, thermal stress, flooding, air quality events and extreme wind (e.g. Bell et al., 2007; Chen, Hill, & Urbano, 2009; Dessai, 2002; Hsieh & Wu, 2012). In many cases the urban environment enhances these risks. For example, urban areas are known to exacerbate heat stress for the following reasons:

- The relatively limited amount of vegetation reduces the opportunity for evaporation and its associated cooling effects, contributing to city temperatures that are typically a few degrees higher than in the surrounding countryside (Howard, 1833; Oke, 1982).
- Paved and built surfaces (e.g. roads, carparks, roofs) are fairly impermeable to water so rainfall is quickly routed into drainage systems and directed away from the surface, thus removing the source of moisture for evaporation (Grimmond & Oke, 1986; Grimmond, Oke, & Steyn, 1986; Oke, 1982; Xiao, McPherson, Simpson, & Ustin, 2007).
- Buildings and roads absorb and store a large proportion of heat during the day and the release of this heat after sunset means temperatures may remain high throughout the night (e.g. Grimmond & Oke, 1999b; Kotthaus & Grimmond, 2014a; Offerle, Grimmond, & Fortuniak, 2005; Roberts, Oke, Grimmond, & Voogt, 2006).
- Dark surfaces (such as asphalt) absorb solar radiation well, and the arrangement of buildings and roads can trap energy, further increasing the heat available (Sailor, 1995; Taha, 1997).
- Human activities provide additional energy: directly through heating buildings and as waste heat from air-conditioning units, electrical appliances, cooking, transportation and human metabolism (e.g. Bergeron & Strachan, 2010; Hamilton et al., 2009; Sailor, 2011). In densely populated areas, this anthropogenic energy supply can be substantial (Ichinose, Shimodozono, & Hanaki, 1999; Klysik, 1996).

Urban design options to moderate heat stress include increasing vegetation cover (e.g. parks, street trees, green roofs), incorporating water bodies or using high albedo building materials (e.g. Lee, Mayer, & Chen, 2016; Nakayama & Fujita, 2010; Ng, Chen, Wang, & Yuan, 2012; Sailor, 1995). Decisions may sometimes have unforeseen and/or detrimental effects. For example, increased use of

* Corresponding author.
E-mail addresses: h.c.ward@reading.ac.uk (H.C. Ward), c.s.grimmond@reading.ac.uk (C.S.B. Grimmond).

http://dx.doi.org/10.1016/j.landurbplan.2017.04.001
Received 8 February 2017; Received in revised form 28 March 2017; Accepted 1 April 2017
Available online 31 May 2017
0169-2046/ © 2017 The Authors. Published by Elsevier B.V. This is an open access article under the CC BY license (http://creativecommons.org/licenses/BY/4.0/).

air-conditioning in warm conditions releases additional waste heat into the environment, further augmenting temperatures and exacerbating heat stress, and putting pressure on power supplies (de Munck et al., 2013; Ohashi et al., 2007; Ramamurthy, Li, & Bou-Zeid, 2015). To lower carbon emissions, one way to encourage use of public transport over private cars is to increase the cost of residents' parking permits. In London, this has led to more people paving over their front gardens so they can park off-road (GLA, 2005b). Vegetation and pervious gravel/soil surfaces have been replaced by impervious concrete or asphalt, enhancing runoff and reducing infiltration of rain water, with the result that evaporation is restricted.

Biophysical models use information about the urban surface (e.g. land cover, building height, radiative properties such as albedo or reflectivity) and inhabitants (population density, energy use), along with past, present or predicted meteorological data to simulate components of the energy balance and/or water balance and thus inform about the environmental conditions. In addition to identifying regions with the greatest risk of exposure, models can also indicate how the risk may change over time. The physical processes represented in models enable us to understand why the risk may be greater under certain conditions and, conversely, to identify measures that may be used to reduce exposure. Models permit the advantages and disadvantages to be explored to better inform planning decisions before investments are made. For example, the impact of several urban cooling measures (including water, vegetation, high albedo surfaces and building dimensions) on pedestrian thermal comfort was assessed for a district in Toulouse that will soon undergo redevelopment (Martins et al., 2016). Potential feedbacks resulting from decisions (made by citizens or government) can be assessed. In the Toulouse study, the high albedo scenario was found to negatively impact pedestrian comfort as more radiation was reflected from walls towards pedestrians.

Understanding and managing climate-related risks in cities is of prime importance, particularly as more variable and more extreme weather is expected in future (IPCC, 2012). The focus of this study is Greater London, home to more than 8 million people (ONS, 2011) and with a daytime population (including workers and tourists) in excess of 10 million (GLA, 2013). The Greater London region is divided into 33 districts: 32 boroughs plus the City of London. For brevity, we refer to all 33 subdivisions as boroughs. There are 12 inner boroughs (plus City of London) and 20 outer boroughs (Fig. 1). Each borough is governed by a borough council (the City of London is governed by the City of London Corporation), responsible for education, provision of services and urban planning. Some planning decisions are also made by the Greater London Authority, responsible for London as a whole. The boroughs represent useful units in terms of governance and the availability of socio-economic data (such as poverty, health status and access to services) which can be used to gauge vulnerability (e.g. Wolf & McGregor, 2013). In future, borough-level risk estimates could be combined with socio-economic data in a move towards interdisciplinary modelling of cities that involves social, economic and biophysical aspects of the city system (Masson et al., 2014). This would enable adaptive or coping strategies to be targeted towards exposed areas that are most vulnerable.

Numerous indicators exist to describe thermal (dis)comfort (de Freitas & Grigorieva, 2015), usually based on temperature and often modified according to some combination of humidity, wind speed, radiation receipt or other variables in an attempt to account for the physiological and psychological effects that translate the physical air temperature to thermal comfort experienced by humans (Johansson, Thorsson, Emmanuel, & Krüger, 2014). Well-known examples include the physiological equivalent temperature (Höppe, 1999), mean radiant temperature (Thorsson et al., 2014) and universal thermal climate index (Jendritzky, de Dear, & Havenith, 2012). Mesoscale modelling studies often rely on 2 m air temperature output, sometimes combined with humidity, to represent human comfort (e.g. Theeuwes, Solcerová, & Steeneveld, 2013). Remotely sensed land surface temperature (Wolf & McGregor, 2013) or urban heat island intensity (Tomlinson, Chapman, Thornes, & Baker, 2011) products are also used. Alexander, Fealy, & Mills (2016) considers the impact of urban development in terms of the surface energy balance. Certain indicators may be more or less suited to particular applications, depending on spatial scale, period of interest and data available. Microscale studies may consider differences between sunlit and shaded areas around individual buildings (e.g. Lindberg, Holmer, & Thorsson, 2008; Middel, Häb, Brazel, Martin, & Guhathakurta, 2014), whereas the computational demands of mesoscale simulations usually restrict the study period to a few days for typical grid-box sizes. A more user-friendly approach is adopted in this study to examine how London's climate responds at the local-scale to changes in meteorology, urban design and policy.

The objectives of this paper are: (i) to assess the response of the urban environment across Greater London to changes in surface characteristics, population and energy use; (ii) to explain the routes by which these changes affect the urban climate; (iii) to demonstrate a methodology which could subsequently be applied to other cities.

2. The biophysical model

2.1. Model description

This study uses the Surface Urban Energy and Water balance Scheme (SUEWS), which has already been evaluated against observational datasets at two urban sites in this region (Ward, Kotthaus, Järvi, & Grimmond, 2016). SUEWS considers the urban surface comprised of seven surface types (paved surfaces, buildings, evergreen trees and shrubs, deciduous trees and shrubs, grass, bare soil and open water) with a single-layer soil store beneath each surface (except water). The exchange of energy at the surface is written (Oke, 1987):

$$Q^* + Q_F = Q_H + Q_E + \Delta Q_S. \quad (1)$$

Q^* is net all-wave radiation; Q_F is anthropogenic heat flux, i.e. the additional energy supplied through human activities. These inputs heat the air (Q_H, turbulent sensible heat flux), evaporate water (Q_E, turbulent latent heat flux) or are stored in (and later released from) the urban volume (ΔQ_S, net storage heat flux). The storage heat flux is calculated using the Objective Hysteresis Model (OHM, Grimmond, Cleugh, & Oke (1991)). Evaporation is calculated using an adapted Penman-Monteith equation (Grimmond & Oke, 1991) with surface conductance formulated after Jarvis (1976), Ward et al. (2016a). A running water balance is calculated at each time-step, providing soil moisture, runoff and surface wetness. Further details can be found in Järvi, Grimmond, and Christen (2011), Järvi et al. (2014) and Ward et al. (2016a).

One of the advantages of SUEWS is its simplicity. High-performance computing is unnecessary, even when running the model for multiple years or multiple areas. Required inputs include information about the surface characteristics (e.g. land cover, building height, albedo, emissivity) and human behaviour (energy use, water use, population density), along with basic meteorological data: incoming shortwave or solar radiation ($K_\downarrow$), air temperature (T_{air}), relative humidity (RH), barometric pressure (p), wind speed (U) and precipitation (P). The versatility of the model allows additional input information to be accepted if available (Lindberg, Grimmond, Onomura, & Järvi, 2015), otherwise recommended values should provide a reasonable approximation in many cases (Ward, Järvi, Onomura, & Lindberg, & Grimmond, 2016). Key site-specific information may need to be derived from other sources (Section 3.1).

The model runs in this study were performed using SUEWS v2016a (Ward et al., 2016b). Here, we focus on the modelled energy fluxes (Eq. (1)). Results are presented in terms of the energy partitioning using the median midday (1100–1400) Bowen ratio (Q_H/Q_E), β_{MM}. Several studies have concluded that the balance between evaporation and

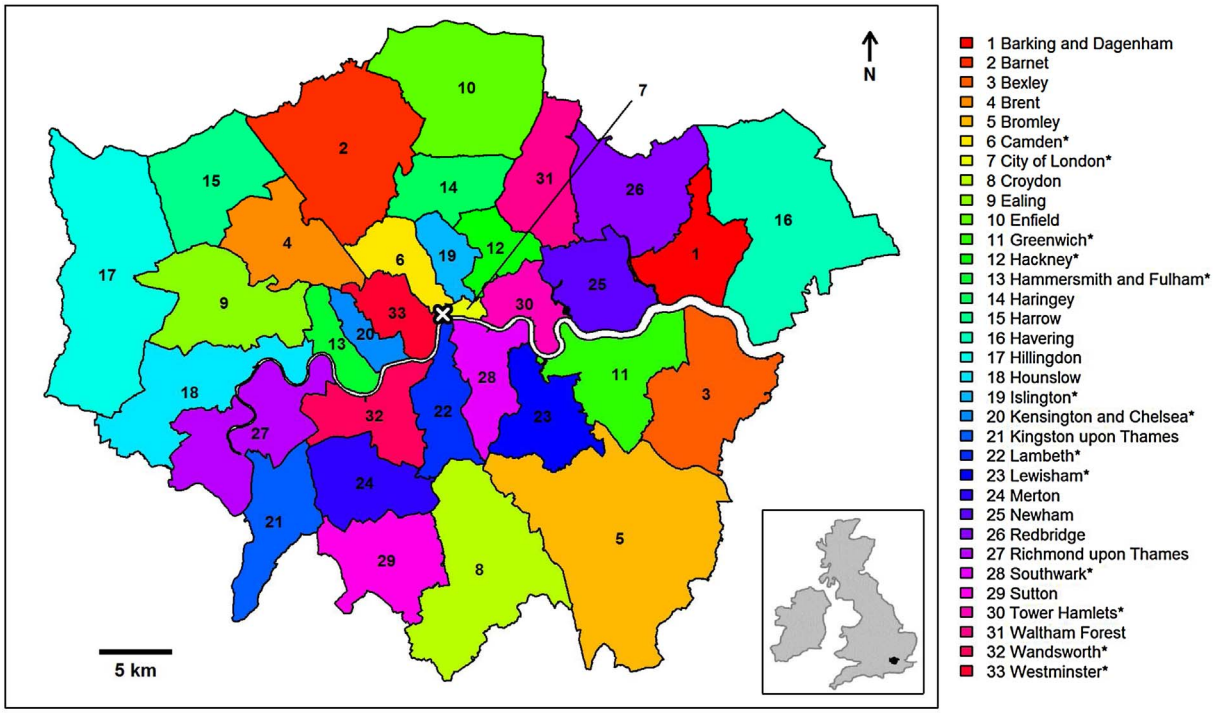

Fig. 1. Greater London boroughs, location of the central London measurement site (cross) and location of Greater London within the British Isles (inset). Asterisks denote inner boroughs. Contains National Statistics and Ordnance Survey data © Crown copyright and database right 2012.

sensible heat flux is a key factor influencing elevated urban temperatures and contributing to the urban heat island (Fischer, Seneviratne, Lüthi, & Schär, 2007; Li and Bou-Zeid, 2013; Li et al., 2015). The less energy used for evaporation, the more energy is available for heating the atmosphere and augmenting air temperatures, i.e. greater risk of thermal stress. Since β_{MM} includes Q_H and Q_E, it will respond to changes in the surface energy partitioning which result from meteorological conditions (including temperature and humidity), surface water availability, additional energy supplied by anthropogenic activities, land cover characteristics, properties of surface materials and state of vegetation. This approach can therefore be used to summarise the impact of a range of urban development or climate mitigation strategies on urban climate.

2.2. Model evaluation

Model output should always be interpreted with care, especially when applied to a region or conditions that differ from those for which the model has been tested. The year-round performance of SUEWS was recently evaluated using observational datasets collected in central London, UK, and suburban Swindon (a large town located about 120 km to the west of London) during the period 2011–2013. We are therefore able to present this application of the model across Greater London with a thorough understanding of its performance. To set the model results in context, values from the observed datasets are provided where available. These are denoted 'OBS URB' for the dense urban central London site and 'OBS SUB' for the suburban residential Swindon site. The UK evaluation demonstrated good performance in summer, particularly for the suburban site, but highlighted two issues. Firstly, there is insufficient information to enable the OHM coefficients used to calculate the storage heat flux to account for building volume or density of building materials, with the result that ΔQ_S is underestimated and Q_H overestimated at URB. Secondly, evaporation from open water is likely overestimated, contributing to a modelled Q_E that is too high. The reader is referred to the full evaluation paper for detailed discussion (Ward et al., 2016a).

In addition to the UK evaluation, SUEWS has also been evaluated against observations at suburban sites in Los Angeles and Vancouver, North America (Järvi et al., 2011); for residential areas of cold-climate cities in Helsinki and Montreal (Järvi et al., 2014); also at a city-centre site in Helsinki (Karsisto et al., 2015); and at an urban and suburban site in Dublin (Alexander, Mills, & Fealy, 2015). These studies demonstrate that SUEWS generally reproduces reasonable results, particularly for suburban areas during summer months. In dense urban areas the large magnitude and considerable spatial variability of Q_F presents a challenge to both modelling and measurement, so uncertainties are largest in these areas. In general, as for the UK sites, ΔQ_S appears to be underestimated for dense urban areas (Järvi et al., 2014). As Q_E is often small in city centres it can be difficult to measure and model accurately (Karsisto et al., 2015; Kotthaus & Grimmond, 2014a). These are fairly typical issues encountered by modellers and urban climatologists, as opposed to particular limitations of SUEWS.

3. Methodology

An objective here is to demonstrate a methodology for locations lacking detailed information. Thus, the model runs have been carried out using readily available information. One advantage of SUEWS is its relatively undemanding input requirements, but appropriate meteorological forcing data, representative surface cover and reasonable estimates of energy use are important.

The flexibility of SUEWS allows the user to define model grids (e.g. to reflect data availability and areas of interest). The focus of this work is at borough-level, but different areas can be specified depending on the application. Each borough is treated as a separate model grid and, at this coarse scale, there is no interaction between grids. The approximation has been made that all boroughs experience the same meteorological forcing, but surface characteristics must be specified individually for each borough.

To give an idea of the summertime behaviour under different conditions, data for the month of July in two consecutive years (2011, 2012) with very different rainfall patterns are analysed. 2011 was a dry year (602 mm rainfall, 76% of the 1981–2010 Normal for southern England), whereas 2012 was very wet (1047 mm rainfall, 132% of the

Normal) (Met Office, 2016). SUEWS is run from 1 January for the two years of interest, allowing several months' spin-up prior to the July study periods. The model setup and parameters are essentially the same as for the evaluation in central London (Ward et al., 2016a), except for the meteorological forcing data and site-specific input.

3.1. Preparation of input information

3.1.1. Meteorological forcing data

The required meteorological forcing is provided by the WFDEI global data product (Weedon et al., 2014), available at 0.5° × 0.5° resolution at 3-h intervals for 1979–2012, downscaled to the model time-step (5-min). Differences in incoming shortwave radiation, rainfall and relative humidity result in small differences when using WFDEI instead of observed data: Q^* is overestimated but the impact on the heat fluxes is reduced by compensating effects (see Appendix A).

3.1.2. Surface cover fractions

Neighbourhood Statistics (NeSS, 2014) provides land cover data for each borough based on the Generalised Land Use Database (GLUD). The most recent 2005 dataset is used here. The following additional information is used to convert the GLUD classes (domestic buildings, non-domestic buildings, road, path, rail, domestic gardens, greenspace, water, other land uses, unclassified land) to the SUEWS land cover classes (Section 2.1):

(i) A breakdown of land cover types within gardens for 2006–8 (Smith et al., 2011)
(ii) Total tree cover in London is 20% (GLA, 2005a)
(iii) It is assumed 20% (80%) of trees are evergreen (deciduous).

Thus, domestic gardens are split up into land cover types using (i); the total proportion of trees (ii) in greenspace plus gardens is used to deduce the proportion of greenspace that is grass; road, path and rail are counted as paved surfaces; other land uses and unclassified land are counted as bare soil surfaces.

Surface cover varies widely across London (Table 1, Fig. 2). City of London has the highest proportion (70%) of impervious surfaces (45% buidings, 25% paved surfaces), followed by Kensington and Chelsea, Islington, and Westminster (60%). These are also the least vegetated boroughs (City of London has only 5% vegetation), along with Tower Hamlets which has the highest proportion of water (22%). The outer boroughs are much more vegetated, with agricultural land towards the edge of the city, open greenspace (parks and commons) and large gardens. Bromley and Havering comprise over 70% vegetation. The spatial variability within boroughs tends to be most pronounced in central London, for example Westminster contains two large parks (Hyde Park and Regent's Park) but is very densely built-up outside these areas. The outer boroughs are predominantly suburban. Substantial water bodies include the River Thames which runs through the centre of London, as well as other open water (lakes, reservoirs, docks) in Tower Hamlets, Waltham Forest and Enfield, for example. The boroughs range in size from 150 km^2 (Bromley) to 12 km^2 (Kensington and Chelsea) (City of London is 3.3 km^2).

The observation site URB is located in a very densely built up area of Westminster borough, close to the boundary with City of London (Fig. 1). The proportion of paved and building surfaces at the URB site (81%) is greater than the borough averages. The proportion of vegetation (5%) is similar to City of London and the proximity to the river means 14% of the source area is made up of open water. The URB site thus represents amongst the most densely built up, least vegetated, and highly populated areas of London. The observation site SUB is more similar to the average values, with 45% vegetation and 49% impervious surfaces. For more details about the observation sites see the original references for these datasets (Kotthaus & Grimmond, 2014a, 2014b; Ward, Evans, & Grimmond, 2013).

3.1.3. Surface characteristics

Characteristics for each surface type are, in this application, assumed to be the same for all boroughs (Table 2). In reality, the variety of building materials will lead to differences in surface properties at the neighbourhood scale or below. The values selected are representative of the surfaces in general (e.g. buildings in European cities) and are the same as those used for the model evaluation.

Building height is estimated at 6.5 m for outer boroughs, 10.0 m for inner boroughs, 20.0 m for Westminster and 25.0 m for City of London (based on Lindberg & Grimmond (2011)). Tree heights are estimated as function of building height (Lindberg & Grimmond, 2011). Roughness length and displacement height are calculated within SUEWS using the rule-of-thumb (Grimmond & Oke, 1999a). Other required characteristics are assumed to be the same across London as public quantitative data are unavailable. Ward et al. (2016a) shows that surface cover and energy use play important roles in surface energy partitioning, whereas building height and small differences in meteorology generally have little impact on model output.

3.1.4. Anthropogenic energy use

The anthropogenic heat flux Q_F can either be provided as input time-series data or calculated within SUEWS. Here, Q_F is calculated within SUEWS to enable values to respond to changes in temperature, population or energy-use characteristics for different scenarios.

SUEWS calculates Q_F based on heating degree days (HDD), cooling degree days (CDD) and population density, ρ_{pop}, (Järvi et al., 2011; Sailor & Vasireddy, 2006):

$$Q_F = \rho_{pop}[a_{F0} + a_{F1}CDD + a_{F2}HDD], \quad (2)$$

where $a_{F0,1,2}$ are coefficients related to non-temperature dependent energy use, building cooling and building heating, respectively. These coefficients can be specified individually for weekdays and weekends and for each model grid. Alternatively generic coefficients could be used for particular land use types (e.g. residential, commerical).

Population data from the 2011 census (ONS, 2011) are used here. The average of the workday and resident (night-time) population is used as some boroughs have a low resident population but very large workday population, particularly in central London (Table 1, Fig. 3a). The same $a_{F0,1,2}$ coefficients are used for all boroughs with separate values for weekdays and weekends. The coefficients were informed by the GreaterQF model (Iamarino, Beevers, & Grimmond, 2012) (Appendix B). Compared to GreaterQF, this approach underestimates Q_F by about 30 W m^{-2} (≈20%) for City of London and by about 10 W m^{-2} for Kensington and Chelsea and Westminster, and is within about 3 W m^{-2} for most other boroughs. Modelled Q_F varies considerably between boroughs (Fig. 3b), with mean annual values for 2012 between 3.9 W m^{-2} (Bromley) and 111.7 W m^{-2} (City of London).

In reality, population varies through the day and workers and residents have different energy-use profiles (e.g. Hamilton et al., 2009; Ichinose et al., 1999). SUEWS' simple approach provides an estimate of Q_F from readily available information, but output from more complex models could be included if appropriate. Accurate estimates of Q_F are more important for densely populated areas (where Q_F is large relative to other terms in the energy balance (Eq. (1))) than suburban areas where a rough estimate of 5–10 W m^{-2} may be sufficient.

External water use is assumed negligible as residents in the UK tend to irrigate far less extensively than in climates with hotter drier summers (Alexander et al., 2015; Ward et al., 2016a).

3.2. Model scenarios

Fig. 4 summarises the mechanisms by which model inputs used to describe the urban surface influence the energy fluxes. For example, a change in albedo of building surfaces would directly impact net radiation, which would indirectly impact the storage heat flux and

Table 1
Characteristics of London boroughs and observation sites. *Inner boroughs. See Section 3.1 for data sources.

No.	Borough	ρ_{pop} [ha^{-1}]			Vegetation/inc. water [%]	Impervious [%]
		Day	Night	Mean		
1	Barking and Dagenham	45.51	50.03	47.77	46.52/49.19	39.06
2	Barnet	36.30	41.13	38.72	57.30/57.74	36.67
3	Bexley	27.62	32.60	30.11	45.99/61.50	31.65
4	Brent	64.38	71.85	68.12	39.19/40.47	50.27
5	Bromley	17.93	20.60	19.27	71.06/71.36	24.99
6	Camden*	175.92	100.92	138.42	35.64/36.49	54.82
7	City of London*	1076.29	22.04	549.17	4.90/18.23	69.59
8	Croydon	35.97	42.08	39.03	55.76/55.87	38.71
9	Ealing	55.19	61.04	58.12	45.43/46.17	44.69
10	Enfield	34.18	38.11	36.14	57.97/62.95	30.97
11	Greenwich*	46.57	53.18	49.87	47.58/49.25	39.59
12	Hackney*	121.35	129.22	125.29	33.76/35.94	52.30
13	Hammersmith and Fulham*	118.00	103.80	110.90	28.80/35.54	52.86
14	Haringey	71.59	86.25	78.92	40.64/41.39	51.14
15	Harrow	39.41	47.40	43.41	54.32/54.69	39.94
16	Havering	18.61	21.14	19.87	70.39/71.81	23.68
17	Hillingdon	26.71	23.70	25.20	59.80/62.81	26.25
18	Hounslow	45.11	44.78	44.95	51.86/55.10	35.48
19	Islington*	179.79	138.91	159.35	23.59/23.86	62.92
20	Kensington and Chelsea*	156.72	128.29	142.50	25.06/27.53	64.06
21	Kingston upon Thames	40.43	42.98	41.71	54.01/54.74	39.00
22	Lambeth*	101.61	112.33	106.97	32.02/32.94	56.58
23	Lewisham*	62.07	78.33	70.20	40.22/40.62	50.84
24	Merton	45.33	53.23	49.28	50.03/50.77	41.14
25	Newham	75.90	83.65	79.78	33.45/38.84	44.43
26	Redbridge	41.22	49.35	45.29	56.21/57.42	37.45
27	Richmond upon Thames	28.37	31.94	30.15	61.78/66.34	28.39
28	Southwark*	111.12	98.72	104.92	34.93/36.95	49.17
29	Sutton	37.42	43.20	40.31	51.65/52.16	40.23
30	Tower Hamlets*	149.21	102.97	126.09	19.38/41.61	42.32
31	Waltham Forest	55.79	66.59	61.19	45.27/51.05	41.38
32	Wandsworth*	70.64	88.09	79.36	39.16/40.91	49.42
33	Westminster*	310.40	98.76	204.58	26.00/31.17	60.05
OBS	URB	310.40	98.76	204.58	5.00/19.00	81.00
OBS	SUB	16.77	47.63	32.20	45.00/45.00	49.00

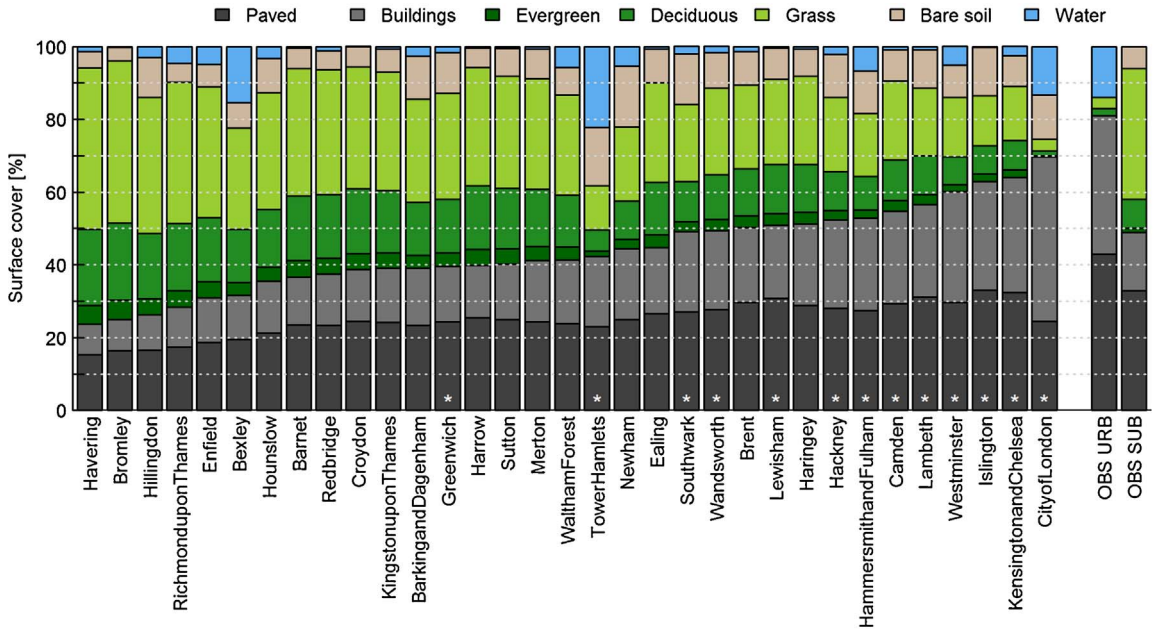

Fig. 2. Surface cover for each borough, in order of increasing impervious (paved + building) fraction, and for the urban (URB) and suburban (SUB) observations (OBS). Asterisks denote inner boroughs. See Section 3.1.2 for data sources.

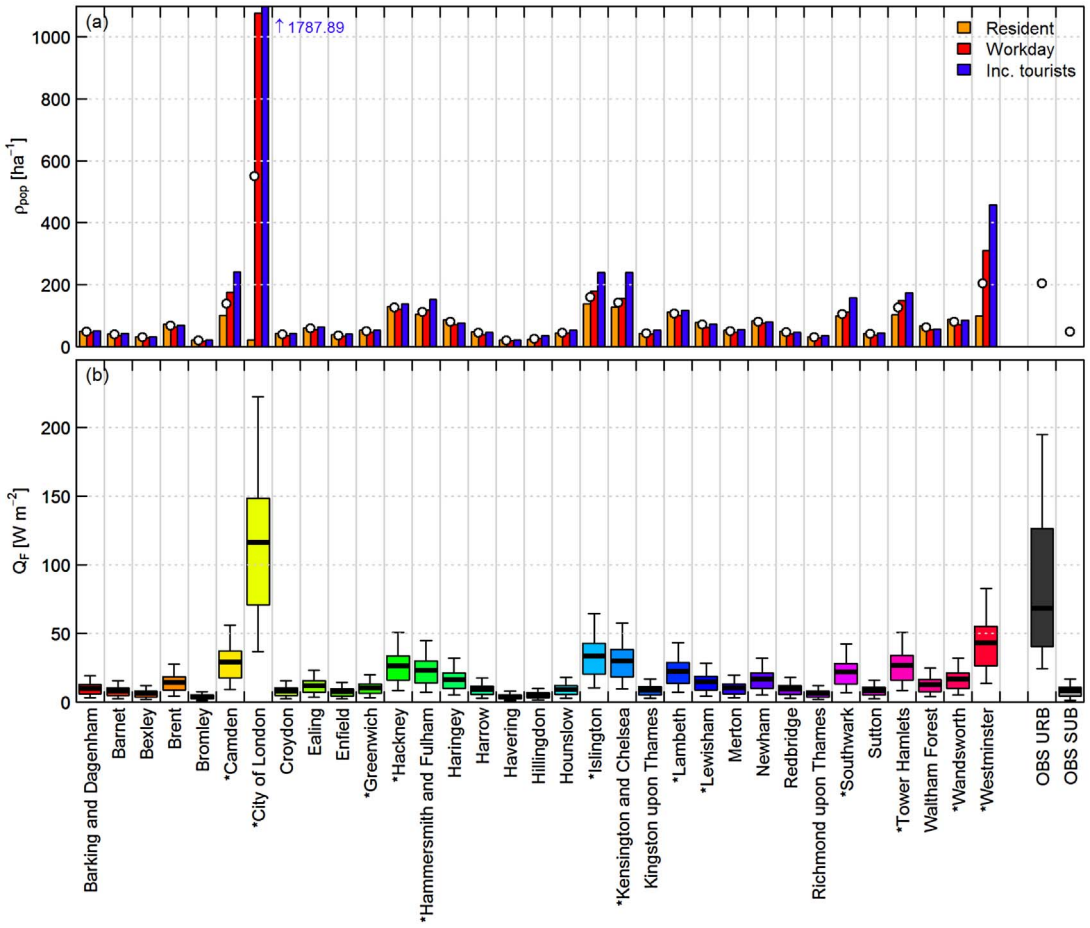

Fig. 3. (a) Population densities by borough: resident (ONS, 2011), workday (ONS, 2011) and daytime including tourists (GLA, 2013). Points indicate values used for the base run. (b) Anthropogenic heat flux for 2012 for each borough modelled by SUEWS and calculated for URB and SUB (see Kotthaus and Grimmond (2014b) and Ward et al. (2013) for details).

alter the available energy, modifying sensible and latent heat fluxes. Thus, changes to the urban system associated with urban development or mitigation measures are communicated to the model by modifying the input information. Model output from these 'alternative scenarios' are then compared to the 'base run' (input data as described in Section 3.1).

Several example scenarios based on real situations have been developed to illustrate the versatility of this approach (Table 3)

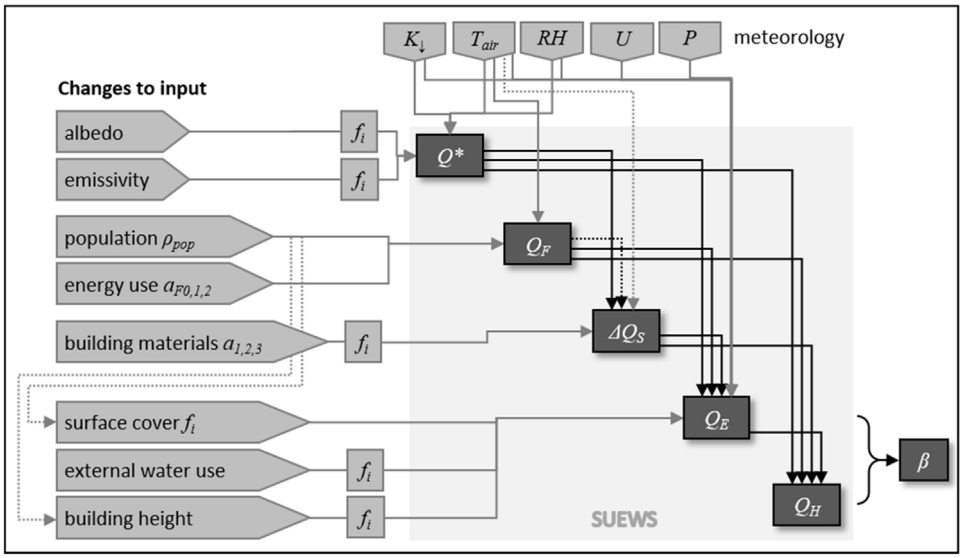

Fig. 4. Flowchart illustrating how changes to the urban landscape are communicated as input to the SUEWS model and the routes by which those changes affect the energy partitioning. Dotted lines indicate possible linkages: an increase in population density may require additional building which changes the surface cover and/or building height; in the current setup Q_F does not impact ΔQ_S, but T_{air} indirectly impacts ΔQ_S via selection of the summer or winter OHM coefficients $a_{1,2,3}$. Surface cover fraction for each surface i is denoted f_i. All other notation is defined in the text.

Table 2
Surface characteristics assigned for each surface type (same as for Ward et al., 2016a). LAI = leaf area index; g_{s_max} = maximum surface conductance.

Surface type	Albedo	Emissivity	Storage capacity [mm]	Wet threshold [mm]	LAI [$m^2\ m^{-2}$]	g_{s_max} [mm s^{-1}]
Paved	0.10	0.95	0.48	0.60	–	–
Buildings	0.12	0.91	0.25	0.60	–	–
Evergreen trees	0.10	0.98	1.30	1.80	4.0–5.1	7.4
Deciduous trees	0.12–0.18	0.98	0.30–0.80	1.00	1.0–5.5	11.7
Grass	0.18–0.21	0.93	1.90	2.00	1.6–5.9	33.1
Bare soil	0.18	0.94	0.80	1.00	–	–
Water	0.08	0.93	0.50	0.50	–	–

Inadvertent climate modification by residents' decisions about their gardens is considered in scenario 1, based on Smith et al. (2011) which describes the actual change in garden composition that occurred between 1998–9 and 2006–8. Scenario 2 considers the Mayor of London's plans for increased tree cover, based on published reports from the Greater London Authority (GLA, 2011). Scenarios 1 and 2 therefore involve changes to the surface cover fractions, f_i. In scenario 3, a 50% reduction in vehicle use is simulated, mimicking similar measures to improve air quality in other cities (e.g. Zhang, Lin Lawell, & Umanskaya, 2017). In scenario 4, an increase in population density is considered, first with no change to the landscape (ρ_{pop} increases directly affecting Q_F, indirectly affecting the available energy), then with associated changes in building density (increased building fraction or building height, directly affecting ΔQ_S and/or Q_E). The required change in building density is estimated using input information for the base run (Appendix C). Scenario 5 combines several measures for climate-sensitive development (reducing energy consumption, increasing vegetation). Finally, the impact of meteorological conditions is explored by running the model with forcing data from 2011 and 2012.

4. Results

4.1. Variability across greater London ('base run')

Fig. 5 shows the modelled β_{MM} values for July 2011/2012. In 2012 values range from 0.41 (Bexley) to 2.71 (City of London). The distribution is positively skewed with values for most (25/33) boroughs below 1.00 and a few higher values: City of London, Islington, Kensington and Chelsea, Westminster. Compared to other summertime study periods, values for July 2012 are generally low reflecting the meteorological and surface conditions (frequent rainfall maintaining moist soils). In July 2011 the range of β_{MM} is greater (from 0.65 (Bexley) to 3.57 (Islington)) and the magnitude is larger for all boroughs except Tower Hamlets (0.75 in 2011, 0.78 in 2012). In both years, inner boroughs tend to have higher β_{MM} than outer boroughs. However, underestimation of Q_F (Section 3.1.4) is thought to result in a slight underestimation in β_{MM} for City of London.

Observational campaigns in urban areas have found that vegetation plays a major role in surface energy partitioning, with increasing vegetation fraction often linked with decreasing summertime Bowen ratio (e.g. Christen & Vogt, 2004; Grimmond & Oke, 2002; Offerle, Grimmond, Fortuniak, & Pawlak, 2006). Primarily, this behaviour is explained by the greater evaporation potential of vegetation and permeable soil surfaces compared to impervious built surfaces. The impervious surfaces tend to have very little capacity to store moisture and thus dry quickly after wetting with most surface water going to runoff which is rapidly removed via pipes and sewerage systems.

SUEWS reproduces this behaviour (Fig. 5a,c): β_{MM} is seen to decrease as vegetation fraction increases. The rate of change is greatest when there is only a small proportion of vegetation. Those boroughs with little vegetation have the highest β_{MM}: City of London, followed by Islington, Kensington and Chelsea, and Westminster (numbers 7, 19, 20 and 33 in Fig. 5a,c). At the other end of the spectrum, Bromley (5) and Havering (16) are ≥70% vegetation and have low β_{MM}. The observed values (URB and SUB in Fig. 5a,c) demonstrate that the model is performing reasonably. Bexley (3) and Tower Hamlets (30) both have notably low β_{MM} given their vegetation fractions because these boroughs contain a significant proportion of open water (Fig. 2), which, according to the model, can evaporate freely. Note that comparison of modelled and observed values at the URB site suggested that SUEWS probably overestimates evaporation from open water (Ward et al., 2016a), however this is a topic of ongoing research since is it is not currently clear whether the depth of the River Thames constrains its temperature and restricts evaporation, or whether considerable evaporation from the river is taking place but is not detected at the height of the sensor (Kotthaus and Grimmond, 2014b). In Figs. 6 and 7 β_{MM} is instead plotted as a function of the proportion of vegetation plus water area.

The robustness of these results is assessed by comparing the monthly average β_{MM} with daily values (Fig. 6a). Generally, the results

Table 3
Assumptions and changes made to the model input for the various scenarios.

	Scenario	Changes to input
1	Garden composition	Surface cover fractions adjusted to represent 1998–9 instead of 2006–8 garden composition.
2i	Increasing tree cover (on paved)	Tree cover increased by 25% in each borough with a corresponding reduction in paved surfaces.
2ii	Increasing tree cover (on grass)	Tree cover increased by 25% in each borough with a corresponding reduction in grass surfaces.
3	Reducing road traffic	Coefficient a_{F0} re-derived having reduced the contribution of vehicle energy use by 50%.
4i	Increasing population (no building)	Population increased to 2020 projection but with no change in land cover (i.e. no new building occurs).
4ii	Increasing population (with building)	Population increased to 2020 projection and homes are built on available land (i.e. vegetation and bare soil surfaces).
4iii	Increasing population (with building)	Population increased to 2020 projection and homes are built on bare soil/unmanaged land only (i.e. no loss of vegetation).
4iv	Increasing population (with building)	Population increased to 2020 projection and homes built upwards only (i.e. building height increased but surface cover fractions unchanged).
5	Climate-sensitive adaptation	Coefficient a_{F0} and a_{F2} adjusted to reflect reduced building energy use by 20%. Coefficient a_{F0} adjusted to reflect reduced vehicle energy use by 10%. Tree cover increased by 25% with a corresponding reduction in paved surfaces for inner boroughs. 25% of bare soil surfaces changed to grass for wealthy boroughs.

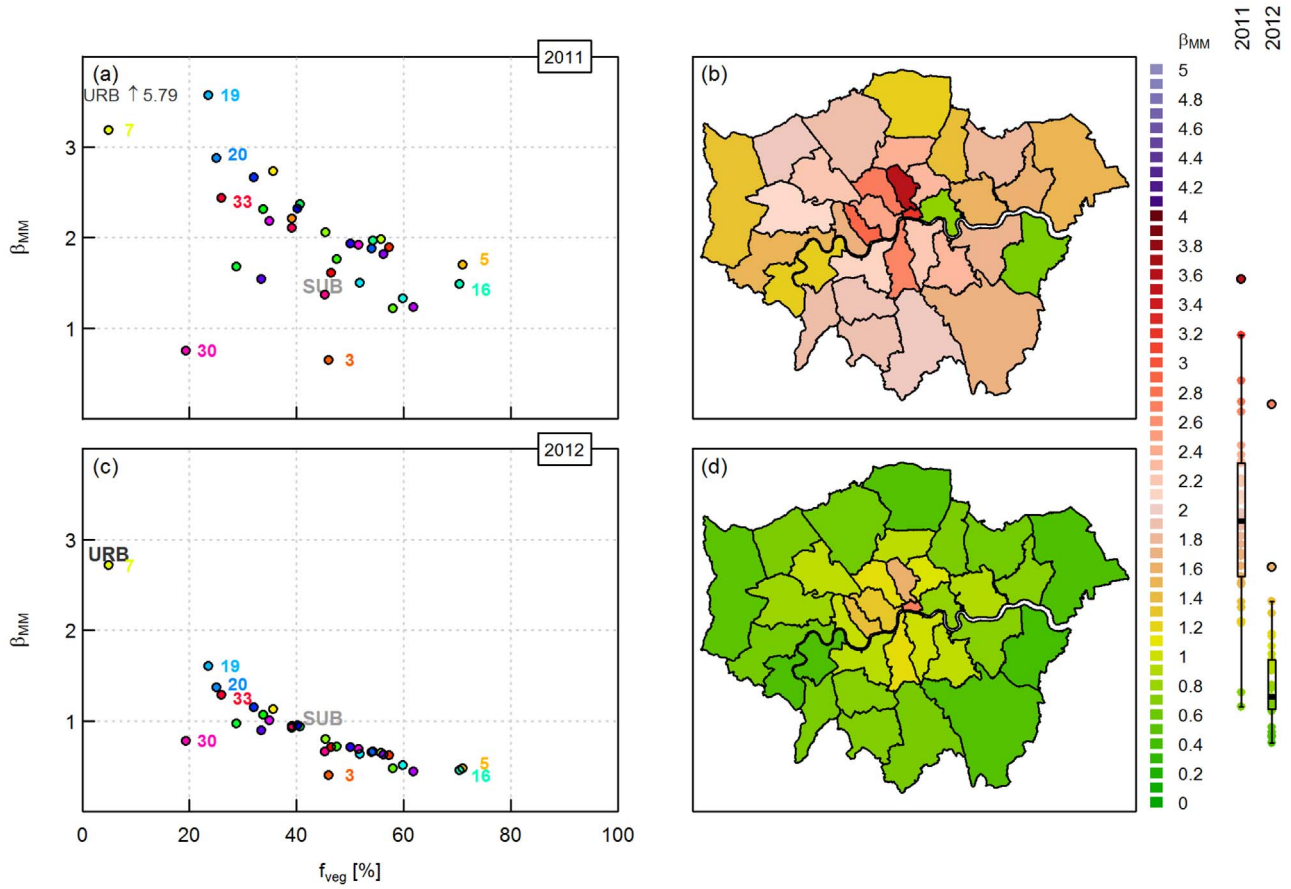

Fig. 5. (a, c) Median midday Bowen ratio β_{MM} as a function of vegetation fraction for the London boroughs and urban (URB) and suburban (SUB) observations. Numerical labels correspond to boroughs (see Table 1). (b, d) Map of β_{MM} for July (b) 2011 and (d) 2012. Boxplots show the inter-quartile range (IQR) with whiskers extending to the furthest point within 1.5× IQR from the upper or lower quartile.

are representative of the daily values, although the range of values increases as β_{MM} increases (also seen in the observations). The few points below 0 occurred on 16 July 2012 which was rainy and overcast so heat fluxes were small. The five-day period 22–26 July 2012, identified as a heat-wave in London (using the method in Li et al. (2015)), had clear-skies, no rain and mean daily temperatures of 21.5 °C (cf. monthly mean daily temperature of 17.0 °C measured at URB). β_{MM} on these heat-wave days (crosses, Fig. 6) is generally higher than on other days (exceptions for Bexley and Tower Hamlets are related to evaporation from water surfaces).

To investigate the relative conditions in each borough, daily β_{MM} values are ranked from 1 (lowest) to 33 (highest) (Fig. 6b). City of London always has the highest β_{MM}, followed by Islington. Although most boroughs change rank with neighbouring boroughs (in terms of rank order, not geographical location) depending on meteorological, surface and sub-surface conditions, the overall ranking remains similar throughout the study period. Exceptions are, again, Bexley and Tower Hamlets. Their substantial water reserves evaporate freely on sunny days with abundant energy whereas evaporation is limited on cloudier days with lower energy input. Therefore, for these boroughs, the sunniest days are those with lower rank positons (e.g. during the heat-wave). Other boroughs with lower rank positions during heat-wave days also contain large areas of water, for example Hammersmith and Fulham, Newham, Waltham Forest, Westminster. Although open water evaporation in SUEWS requires more detailed evaluation, the qualitative result that water bodies help ameliorate heat stress is in agreement with other studies (e.g. Theeuwes et al., 2013).

Results are similar for July 2011, but with more variation in daily values and less consistent rank positions (Fig. 7). Frequent rainfall in 2012 maintains a plentiful supply of moisture: the surface is often wet following rainfall and soils are moist. In 2011, less frequent rainfall allows the surfaces to dry out, reducing evaporation (except where the moisture supply is maintained by large water bodies; those boroughs have notably low rankings in Fig. 7b). This behaviour results in a wider spread of β_{MM} values. That rainfall prompts a sharp decrease in the Bowen ratio followed by an increase as surfaces dry has been demonstrated in observational data (Kotthaus & Grimmond, 2014a; Ward et al., 2013). Differences in evaporation between years can also result from differences in Q^*, but summer 2011 and 2012 were both cloudier than normal (1981–2010).

There is little spatial variation in Q^* between boroughs (Fig. 8). Incoming shortwave ($K_{\downarrow}$) and longwave ($L_{\downarrow}$) radiation are identical for all boroughs as the same meteorological forcing has been assumed (Section 3.1.1). Atmospheric pollution can lead to reduced shortwave radiation receipt in city centres compared to their surroundings (Arnfield, 2003). The size of this reduction is about 10% in London (Ryder and Toumi, 2011) but can be larger for more polluted cities (Jáuregui & Luyando, 1999). Conversely, an increase in $L_{\downarrow}$ is typical due to warmer temperatures and increased pollutant concentration over cities (Arnfield, 2003; Christen & Vogt, 2004). These effects are not simulated here but, to a certain extent, these urban-rural differences in $K_{\downarrow}$ and $L_{\downarrow}$ compensate for each other. The highest Q^* values are thus obtained for the least vegetated boroughs with the lowest bulk albedos ($\approx$0.12) and the lowest Q^* values for the most vegetated boroughs with the highest bulk albedos ($\approx$0.17). Compared to the day-to-day variation in midday Q^*, differences between boroughs are small. This is thought to be realistic as many observational studies report little difference in Q^* between urban and rural sites or multiple sites within a city (e.g. Christen & Vogt, 2004; Schmid, Cleugh, Grimmond, & Oke, 1991). For higher resolution studies, albedo could be adjusted to

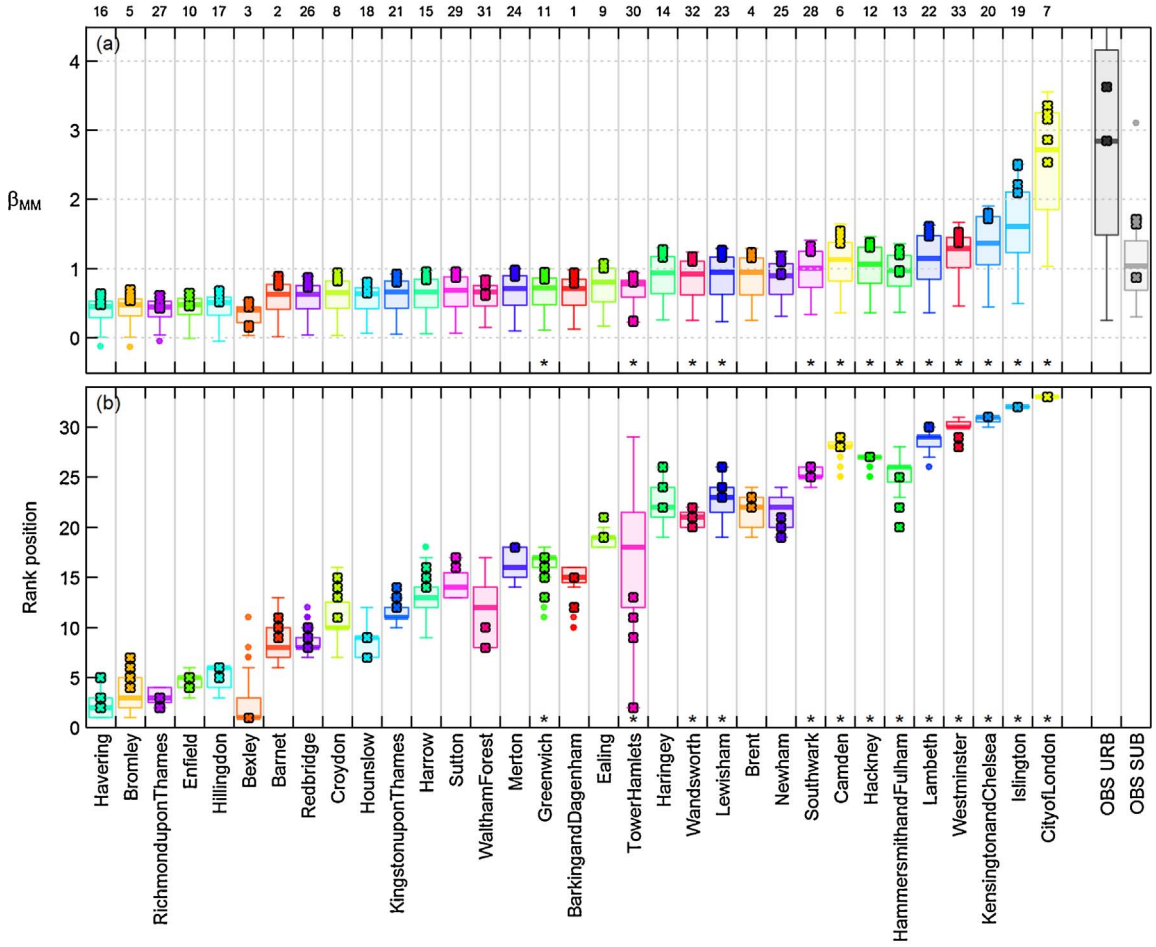

Fig. 6. Boxplots of (a) daily median midday Bowen ratio β_{MM} values and (b) rank (1 = lowest, 33 = highest) during July 2012 for each borough (arranged in order of decreasing fraction of vegetation + water). β_{MM} values are also shown for the urban (URB) and suburban (SUB) observations (OBS). Crosses represent values on heat-wave days (22–26 July 2012). Numerical labels along the top are as given in Table 1.

incorporate the effect of shading (Sailor & Fan, 2002) or to represent specific materials (e.g. slate tile versus ceramic tile roofs). Modelled Q^* for all boroughs is larger than the observed values at the evaluation sites, mainly because the WFDEI $K_{\downarrow}$ is higher than the observed values (Appendix A).

For midday in summer, these results suggest the additional energy supplied by anthropogenic activities is about 30% of Q^* for City of London (45% at URB). Q_F can be even more important in winter and at high latitudes. For the most densely populated boroughs, Q_F acts to increase Q_H as Q_E is limited by the low vegetation fraction and lack of available moisture. Thus, boroughs with the highest Q_H tend to be those with the highest Q_F (City of London, Islington, Kensington and Chelsea, Westminster). The difference in energy partitioning between study years can be seen here: Q_H generally exceeds Q_E in July 2011, whereas Q_E exceeds Q_H for the more vegetated boroughs in July 2012 (Fig. 8).

4.2. Model scenarios

4.2.1. Scenario 1: change in garden composition

The composition of gardens in London has changed over recent years (Smith et al., 2011). Compared to 1998-9, gardens in 2006–8 contain more buildings and paved surfaces (41% cf. 31%) and less vegetation (58% cf. 65%). For this first scenario, we assess the impact on local climate by considering the change in β_{MM} if today's (i.e. 2006–8) garden composition was returned to that of 1998-9.

Overall, domestic gardens comprise 24% of the total area of Greater London. The decrease in vegetation fraction associated with the change in garden composition is small for many central boroughs, but for inner boroughs with appreciable amounts of garden (≈20%, e.g. Islington) the small increase in vegetation fraction causes a discernible reduction in β_{MM} (Fig. 9a and b). For the outer boroughs, even though there is a lot of garden space, the already higher vegetation fraction means the change in garden composition generally has a smaller impact. However, all boroughs show a reduction in β_{MM}, indicating that the change in garden composition that has occurred since 1998-9 has altered the surface-atmosphere exchange: nowadays more energy is directed to heating and less to evaporation. Such trends are expected to continue as more people pave their front gardens for parking or opt for low maintenance gardens (GLA, 2005b). Other environmental impacts associated with replacing vegetation with paved surfaces include reduced biodiversity and increased flood risk. SUEWS suggests an increase in annual runoff of 5–15 mm due to this change in garden composition (modelled annual totals for each borough range between 376 and 553 mm in 2012).

The impact of these land cover changes on the surface energy balance can be understood using Fig. 4. Modifying the surface cover fractions changes the bulk radiative properties of the surface. Emissivity has little impact on the output, but vegetation generally has higher albedo than typical materials used for paving or building in the UK (Table 2) so the increase in bulk albedo results in lower Q^*. The anthropogenic heat flux is unchanged by this scenario, but the storage heat flux is reduced (as grass stores less heat than paved and building surfaces, and because Q^* is lower). The increase in vegetation fraction means more of the available energy is used in evaporation, leaving a smaller proportion for the sensible heat flux. Hence Q_E increases and Q_H decreases.

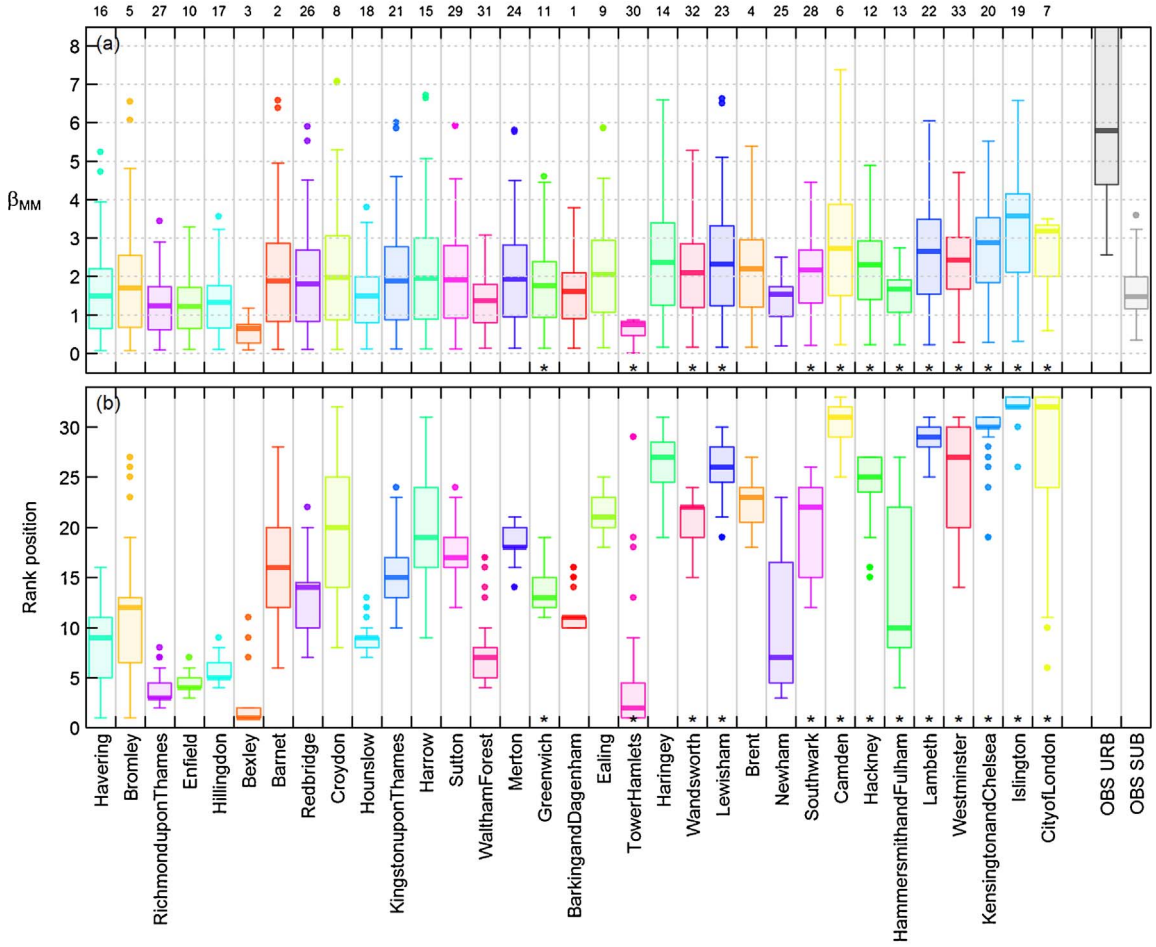

Fig. 7. As for Fig. 6 but for July 2011.

Buildings and paved surfaces tend to store (and later release) a large amount of heat as their constituent materials have high heat capacities. In SUEWS, this behaviour is simulated through different OHM coefficients ($a_{1,2,3}$) for each surface type. However, Ward et al. (2016a) suggests the range of OHM coefficients in the literature may be insufficient to account for the wide range of urban surface types, with the result that ΔQ_S may be underestimated in built-up areas. Central boroughs (City of London, Kensington and Chelsea, Islington, Westminster) have the highest ΔQ_S, but $\Delta Q_{S\ OBS\ URB}$ is much larger (Fig. 8). As previous work accounting for the three-dimensional building volume did not significantly improve the performance of OHM (and decreased performance in some cities) (Grimmond & Oke, 1999b), in the current configuration building height does not affect ΔQ_S, although it is reasonable to expect larger ΔQ_S with greater built volume.

4.2.2. Scenario 2: increase in tree cover

Recognising the benefits of urban trees (e.g. Salmond et al., 2016), the Mayor of London plans to increase London's tree cover from 20% to 25% by 2025 (GLA, 2011). Two scenarios are considered here: (i) trees replace paved surfaces; (ii) trees replace grass surfaces (Table 3). In each case, the input surface cover fractions are altered so that the tree cover increases by 25% for each borough (in line with total tree cover

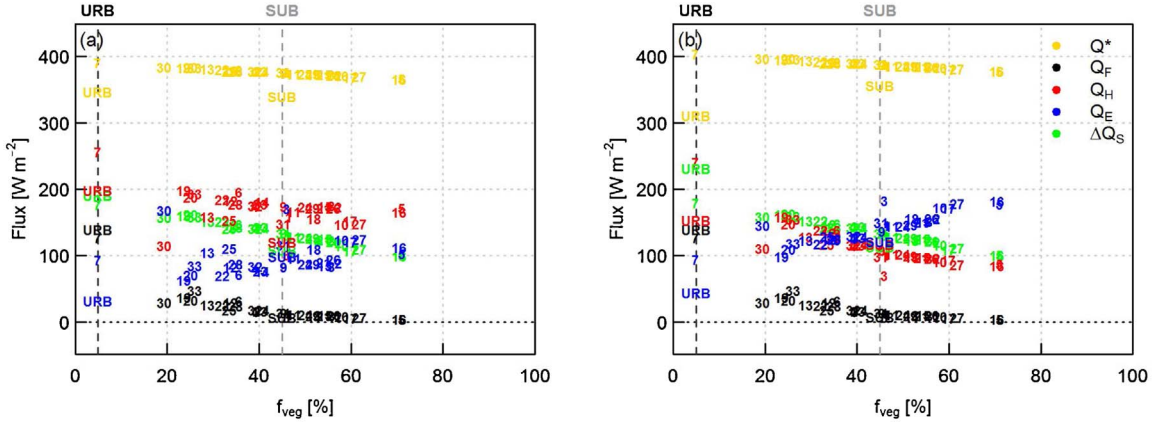

Fig. 8. Energy fluxes (median midday values for July (a) 2011 and (b) 2012) as a function of vegetation fraction for the London boroughs (numbers, as Table 1) and for urban (URB) and suburban (SUB) observations.

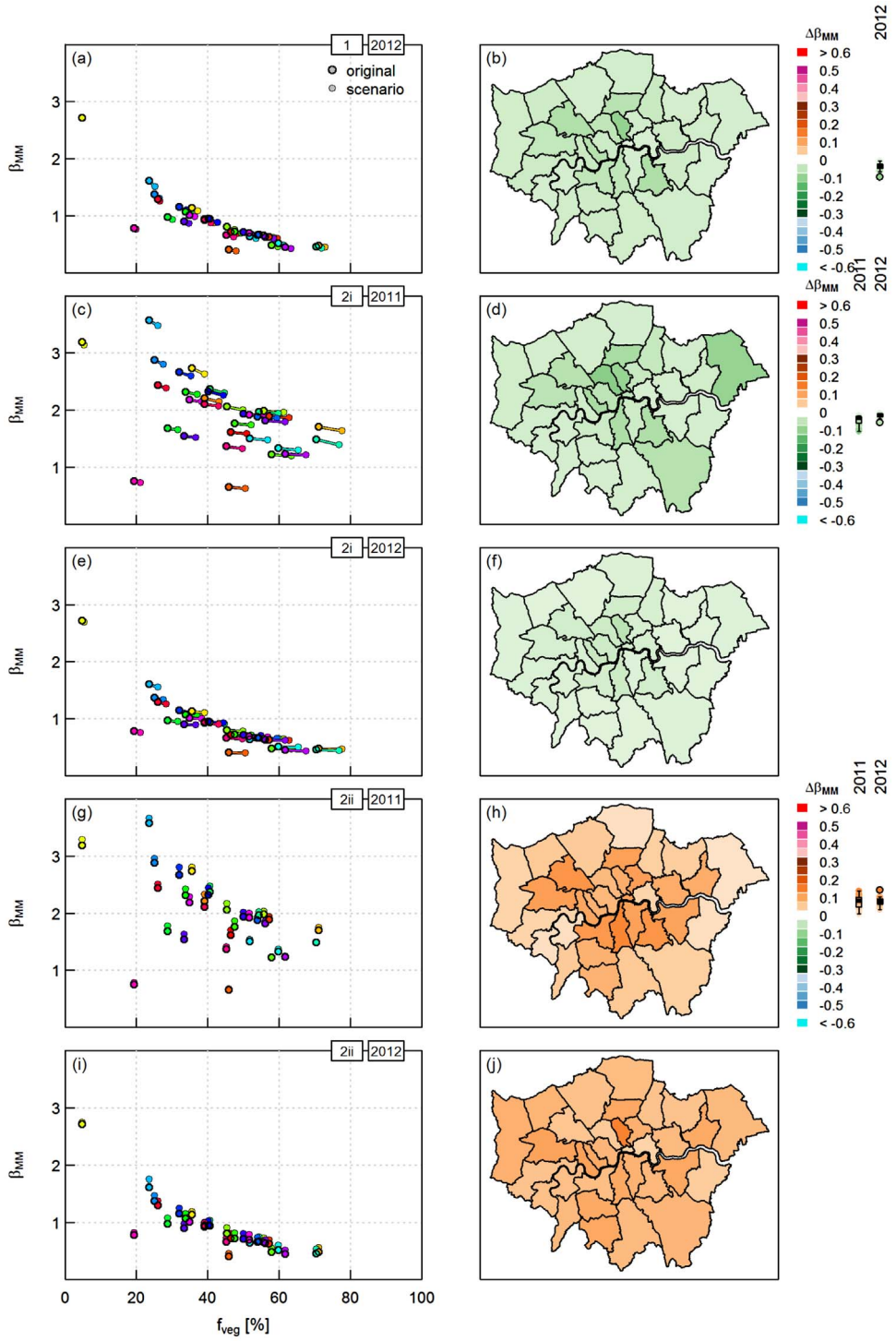

Fig. 9. (a, c, e, g, i) Median midday Bowen ratio β_{MM} as a function of vegetation fraction for the current situation and for scenarios 1 (July 2012) and 2 (July 2011, July 2012); (b, d, f, h, j) map of the change in β_{MM} under each scenario ($\Delta\beta_{MM} = \beta_{MM\ scenario} - \beta_{MM\ original}$). Values for each borough are shown (alongside the legend) with their distribution (boxplot). Scenario 1 assumes a change in surface cover equivalent to returning today's (i.e. 2006–8) garden composition to that of 1998–9. Scenario 2i/2ii constitutes an increase in tree cover with trees replacing paved/grass surfaces. See text for details.

across Greater London increasing from 20% to 25%).

When trees replace paved surfaces β_{MM} decreases across all boroughs (Fig. 9c–f). The largest changes in vegetation fraction occur for boroughs with the largest proportion of trees, but the largest changes in β_{MM} occur where the vegetation fraction is small. The Mayor's Street Tree Programme aims to plant new trees in the most deprived areas, including areas with few street trees (GLA, 2011). Although no borough-scale plans were available, this strategy will be more effective than suggested by scenario 2i, as the rate of change of β_{MM} is greater where vegetation is scarce. The impact is also greater in 2011 than 2012 (mean $\Delta\beta_{MM} = -0.042/-0.018$ in 2011/2012, which corresponds to a change in Q_H and Q_E of around $\pm$ 4 W m^{-2} assuming a Q^* of 400 W m^{-2} and $\beta_{MM} \approx 1$).

If trees instead replace grass surfaces (scenario 2ii) there is no change in vegetation fraction and the results are quite different (Fig. 9g–j). The presence of more trees and less grass lowers the surface conductance, which decreases Q_E and allows Q_H to increase (mean $\Delta\beta_{MM} = 0.072/0.077$ in 2011/2012). In 2011 the impact on the outer

boroughs is less than in 2012 (Fig. 9h, j), possibly because soil moisture (rather than vegetation fraction) plays a significant role in limiting evaporation in dry years. These results highlight the importance of considering both where trees will be planted and what will they replace. Note that the types of vegetation planted/replaced are also relevant. These can be represented in the model by specifying vegetation characteristics (particularly maximum surface conductance).

4.2.3. Scenario 3: reduction in road traffic

Scenario 3 considers a change in human behaviour, without changing the landscape, namely a 50% reduction in vehicle usage. This scenario is intended to represent strict traffic controls enforced to manage air pollution. For example, during the 2008 Beijing Olympics, vehicle use was restricted on alternate days based on odd/even licence plates and vehicles not meeting emission standards were banned completely, which meant only about 40% of vehicles were permitted to use the roads each day (Song & Wang, 2012; Yu, Wang, Zong, Li, & Lü, 2010). As well as the impact on pollutant emissions, there will be an associated reduction in heat emissions.

According to GreaterQF, vehicle use contributes about 15% of total Q_F. To model a 50% reduction in road traffic, the coefficient a_{F0} (see Section 3.1.4) was reduced to 0.1457 and 0.1384 W m^{-2} (cap ha^{-1})$^{-1}$ on weekdays and weekends, respectively. These values were derived using the same method as the generic London borough coefficients (Appendix B) but with the vehicle contribution halved. The reduction in Q_F reduces the energy input to the surface and results in lower β_{MM} (not shown). The impact is generally very small (mean $\Delta\beta_{MM} = -0.012$ in 2012), except for very densely populated boroughs, mainly because building energy use is so high. Policy may therefore be better directed towards reducing building energy consumption. In warmer climates, air conditioning can substantially increase Q_F during summer, maintaining cooler indoor temperatures but exacerbating heat stress outside. Reducing transport use is much more important in terms of air quality (e.g. Beevers & Carslaw, 2005).

4.2.4. Scenario 4: population increase

Scenario 4 considers the impact of population increase. The resident population of Greater London is expected to increase from 8.2 million (ONS, 2011) to 9.1 million by 2020 (GLA, 2014). Here, the percentage projected change in resident population for each borough is applied to the current population densities (Table 1). First, the impact of the additional population alone (i.e. no new building) is considered (scenario 4i, Fig. 10a–d). There is negligible impact for boroughs where ρ_{pop} and Q_F is small (Bexley, Bromley, Havering) or where the change in population is very small (Kensington and Chelsea $\Delta\rho_{pop} = 0.2\%$). For central boroughs, the increase in ρ_{pop} caused an increase in β_{MM}, particularly for City of London ($\Delta\beta_{MM} = 0.155/0.253$ in 2011/2012) where considerable population growth is combined with the already high population density to increase Q_F (although note that part of the reason for this large change is due to the assumption that has been made in scaling the mean of day- and night-time ρ_{pop} by the projected increase in resident ρ_{pop}). The additional population has a larger impact during dry weather as, when water is limited, the extra energy acts to increase Q_H rather than Q_E.

A more realistic scenario also increases the proportion of buildings in order to provide the growing population with somewhere to live and work. The increase in buildings required to match the population growth was calculated from the relation between building fraction and ρ_{pop} fitted to the current values for each borough (Appendix C). In scenario 4ii, the land cover fractions are adjusted to account for this increase in building fraction (the proportion of vegetation and bare soil is reduced accordingly; it is assumed existing paved, building and water surfaces are not available to be built on). In scenario 4iii, the building fraction is increased as for scenario 4ii, but with a corresponding decrease in bare soil surfaces only (i.e. development of unmanaged land rather than removing vegetation). In scenario 4iv, the land cover fractions are unchanged but building height is increased to provide the same new building volume as for scenario 4ii and iii.

Results for scenario 4iv (not shown) are very similar to scenario 4i (within 0.5%) except for Tower Hamlets ($\Delta\rho_{pop} = 32\%$) where β_{MM} increases from 0.78 to 0.81 (scenario 4i) to 0.82 (scenario 4iv). Equivalent values for 2011 are 0.75 increasing to 0.79 and 0.82. These results suggest that building height has a much smaller impact than building extent (assuming roughness length and displacement height scale with mean building height). Note that the parameters within SUEWS were not changed to account for shading or radiation trapping within the urban canyon, both of which increase with building height, reducing daytime Q^* but increasing night-time Q^* (e.g. Mavrogianni et al., 2011).

If building occurs horizontally rather than vertically, the associated loss of vegetation increases β_{MM} (scenario 4ii, Fig. 10e–h), particularly for the inner boroughs and more so for drier years than wetter years. If vegetated areas are protected from development and new buildings are constructed only on bare soil, the impact is generally reduced (scenario 4iii, Fig. 10i–l). This reduction is greater in 2012 than 2011, which again, is probably related to soil moisture availability. The lack of rainfall in 2011 means soil moisture stores are low. When rain does fall, it can directly infiltrate the soil beneath pervious surfaces but not beneath impervious surfaces (SUEWS assumes buildings and paved surfaces are totally impervious). A reduction in pervious surfaces (bare soil and vegetation) reduces infiltration and increases runoff, so the soil receives less water. Therefore, both scenario 4ii and 4iii have a larger impact in 2011 than 2012, as in 2012 soil moisture is higher and less of a limiting factor. Thus, the proportion of vegetation is the important factor in 2012, whilst the proportion of pervious surfaces is important in 2011.

4.2.5. Scenario 5: cimate-sensitive adaptation

Scenario 5 combines several aspects from previous scenarios to assess the potential impact of adapting London in a climate-sensitive way (Table 3) including: reduced anthropogenic energy emissions brought about through improved energy efficiency of buildings and improved access to public transport (see Appendix B); and increased vegetation cover brought about through tree planting in inner boroughs (i.e. focusing on the least vegetated boroughs) and replacing bare soil with grass in wealthy boroughs (assuming wealthy boroughs have the means to develop unmanaged land into green spaces). Wealthy boroughs were identified as those with the top 20% highest median household income (GLA, 2012/3): Kensington and Chelsea, City of London, Westminster, Richmond upon Thames, Camden, Wandsworth.

Scenario 5 results in a reduction in β_{MM} across all boroughs, but the largest changes occur for the inner boroughs (where the proportion of vegetation increases and the considerable anthropogenic heat flux decreases) and wealthy boroughs (where the proportion of vegetation increases) (Fig. 11). The impact is greater in 2011 than 2012. Boroughs classified as both inner boroughs and wealthy boroughs experience the largest change: for Camden, City of London, Kensington and Chelsea, Wandsworth and Westminster $\Delta\beta_{MM}$ exceeds -0.10 (Fig. 12). The decrease in energy use for the outer boroughs (where Q_F is small) has a small impact in 2012 ($\Delta\beta_{MM} < -0.01$ for many boroughs) but has a greater effect in 2011. There would also be a reduction in carbon emissions associated with the decrease in fuel combustion for transport and home heating.

All the scenarios presented here produce a change in the same direction for all boroughs. However, alternative development pathways can be envisaged where the situation improves in some boroughs but worsens in others. For example, population growth accompanied by extensive building in some areas, compared to greening initiatives in other boroughs where there is less pressure on space. Input data can be easily adapted to represent the relevant changes; the demonstrations here are intended to be examples.

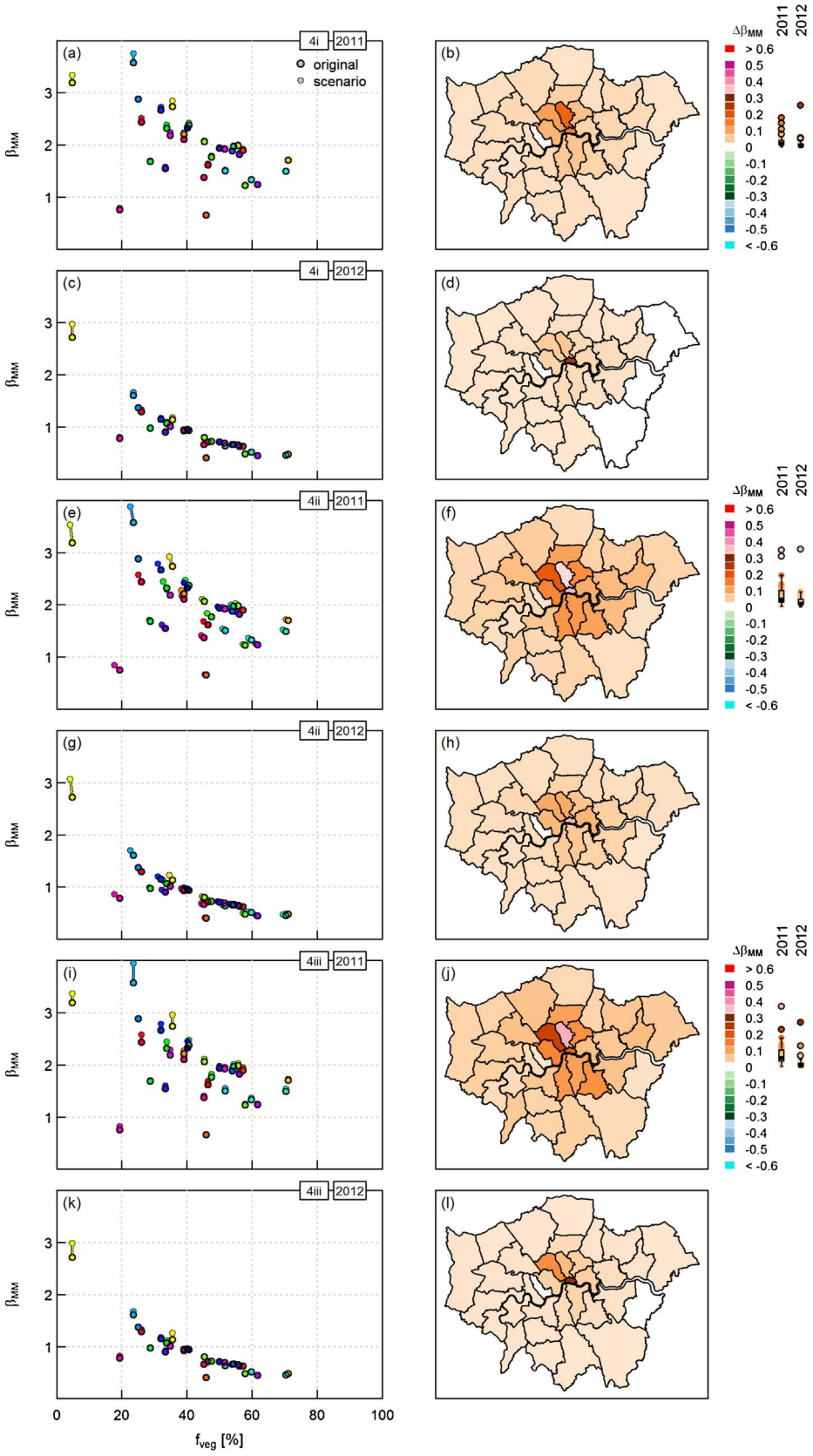

Fig. 10. As for Fig. 9 but for scenario 4i–iii (Table 3). These scenarios assume an increase in population with (4i) no additional building; (4ii) an increase building fraction, with buildings replacing bare soil and vegetation; and (4iii) an increase in building fraction, with buildings replacing bare soil only. See text for details.

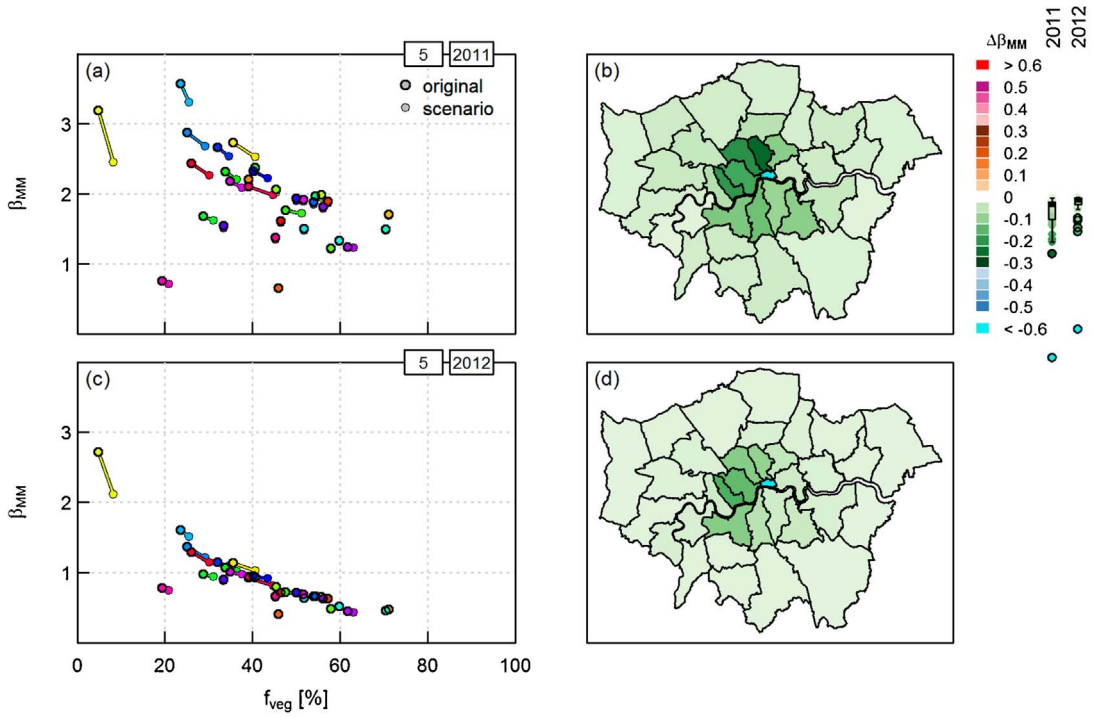

Fig. 11. As for Fig. 9 but for scenario 5. Scenario 5 combines aspects of the previous scenarios to assess the potential impact of adapting London in a climate-sensitive way (see text for details).

5. Summary and conclusions

Numerous policy decisions must be made without knowledge of their outcome. Scenario modelling can help inform about likely (or unintended) outcomes, or can be used to compare likely impacts of one decision versus another. Since all models are approximations of reality they must be interpreted at such, bearing in mind their imperfect representation of physical processes and the assumptions involved in specifying model parameters and required input information. Estimates of these can be made from the literature, datasets or other models and sensitivity studies can be used to assess uncertainties. The decisions involved in implementing environmental measures are significant. For instance, increasing the number of trees could have a different outcome (positive or negative) depending on where and how they are planted and on the species selected. The impact of population growth depends on where and how people will be housed: increasing building height was found to have a much smaller impact than increasing building extent due to the important role of vegetated surfaces in moderating the urban climate. Compact cities may also offer advantages in terms of reduced transport demand (Mills, 2007). The results show that changes in land cover can have major impacts on urban energy partitioning, with the biggest changes tending to occur in the least vegetated areas where heat stress is greatest. In recent years, trends in garden composition (i.e. decisions taken by residents) have resulted in more

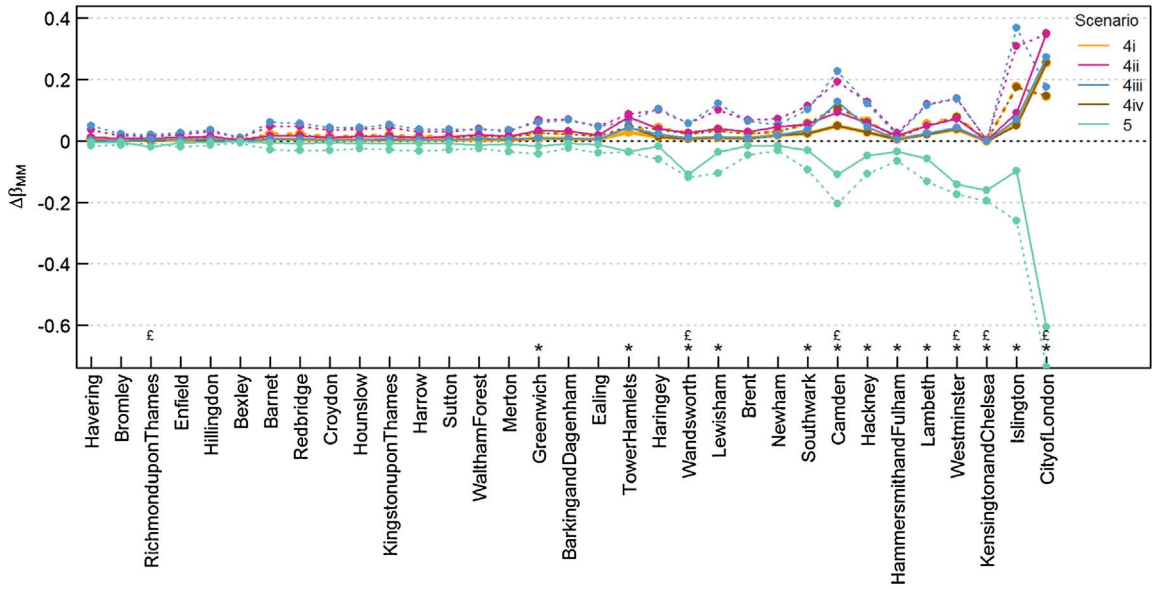

Fig. 12. Change in median midday Bowen ratio $\Delta\beta_{MM}$ for scenarios 4 (increase in population) and 5 (climate-sensitive design) for 2011 (dotted lines) and 2012 (solid lines). Asterisks denote inner boroughs, £ denote wealthy boroughs.

of the available energy being used to heat the atmosphere. Human behaviour has a considerable impact on the environment, particularly in very densely populated areas. However, it should not be overlooked that uncertainties are also greatest for such areas, where fluxes can vary dramatically over short temporal and spatial scales and observations are scarce.

This paper demonstrates how the biophysical SUEWS model can be used to assess the response of the urban climate across a city to various urban development and climate mitigation measures. SUEWS has the capability to use more detailed information when available, for example through consultation with city planners. We describe the approaches taken to convert readily available datasets to the inputs required by the model, with the intention that analyses could be performed at other sites using a similar methodology. In terms of urban design, this study highlights the following:

- (Well-watered) vegetation is a key control on urban energy partitioning and important for moderating elevated urban temperatures
- Consequently, building upwards has a smaller impact on the urban energy balance than building on vegetated areas
- Adding vegetation has greatest impact in sparsely vegetated areas
- A range of meteorological conditions should be considered when assessing the impact of scenarios.

This study overcomes two limitations often encountered when assessing impacts of urban planning scenarios: few models respond to the range of controls assessed here (e.g. surface cover, population density, energy use, building properties); and many studies focus only on a few days due to high computational demands. Furthermore, SUEWS has also been evaluated against energy balance observations in a range of cities. Although model results must be interpreted with care, especially when pertaining to different conditions than those for which the model has been evaluated, ongoing evaluation work will extend the range of conditions and locations for which the model behaviour can be understood. Model development currently underway should improve the capabilities and accuracy of SUEWS, particularly in terms of the storage and anthropogenic heat flux.

This study focuses mainly on the risk of heat stress (with some consideration of hydrology through the water balance, although the water balance has not yet been thoroughly evaluated in the UK). There are also many other environmental factors to consider, such as air quality, noise pollution and biodiversity (beyond the scope of the current study), as well as economic and social factors. To analyse biophysical exposure risk in conjunction with social vulnerability (Birkmann et al., 2015; Birkmann & Welle, 2015), these results could be combined with socio-economic data.

The SUEWS model is available to download from http://micromet.reading.ac.uk.

Acknowledgements

This work was supported by NERC/Belmont TRUC NE/L008971/1 and Newton Fund/Met Office CSSP China. We thank everyone who contributed to data collection and model development, particularly Andy Gabey, Leena Järvi, Simone Kotthaus, Fredrik Lindberg and Zhe Zhang.

Appendix A. Meteorological forcing data from WFDEI

The WFDEI dataset (WATCH Forcing Data methodology applied to ERA-Interim data) (Weedon et al., 2011, 2014) is used to provide the meteorological data required for SUEWS: incoming shortwave radiation ($K_{\downarrow}$), air temperature (T_{air}), relative humidity (RH), barometric pressure (p), wind speed (U) and precipitation (P). Continuous, long-term observational datasets of these variables at sub-daily resolution are extremely rare due to the difficulties of siting instrumentation in urban environments and the workload involved in maintaining high-quality measurements over an extended period. The WFDEI dataset has global coverage (0.5° × 0.5° resolution) and is available at 3-h intervals for the years 1979–2012, allowing analysis of past weather events.

Although Greater London covers about 4 half-degree grid boxes, WFDEI data extracted for the central location of the URB site (51.51° N 0.12° W) are used, i.e. each borough uses the same meteorological forcing data. Differences between the 4 grid boxes were minor; here the single URB grid was chosen to simplify the comparison with observed data.

SUEWS requires input data at 60 min (which are linearly downscaled at the outset to the time-step of the model, here 5 min). Therefore, all variables are first linearly interpolated from the 3-h WDFEI data to 60 min, except 3-h rainfall which is downscaled directly to 5 min accounting for the intermittency of wet periods and conserving the total mass in each 3-h period (Table A1).

Using WFDEI data in place of observations (usually at 1-h resolution) can introduce errors (i) through interpolation of 3-h to 1-h data and (ii) as a result of differences between what the WFDEI and observed dataset represent, namely the height (see Table A1 for WFDEI; 49.6 m for URB), elevation (78 m for WFDEI; 10.7 m for URB) and land use.

To investigate (i), observations from URB (1 h) are averaged to 3 h to represent the resolution of the WFDEI data according to Table A1. That is, $K_{\downarrow}$ is the average of the previous 3 h; T_{air}, RH, p and U are instantaneous values (approximated here by the mean for the current hour and for the following hour). This 3-h dataset is then downscaled to 1 h in the same way as for the WFDEI dataset and compared to the original 1-h observations (Fig. A1). The assumption that the variables change linearly in time results in some scatter, particularly for $K_{\downarrow}$ which can change dramatically over hourly time scales. The diurnal cycle of $K_{\downarrow}$ is also slightly widened and flattened (not shown). The impact on the other variables is small and generally makes no appreciable difference to the model output.

More substantial differences are found between WFDEI and OBS datasets (Fig. A2). $K_{\downarrow OBS}$ is smaller than $K_{\downarrow W1h}$ (mean values for daytime are 195.7 W m^{-2} (at URB) and 220.2 W m^{-2} in 2012). To some extent, this is expected due to attenuation by aerosols over central London (see Section 4.1), but comparison between WFDEI and OBS data for the SUB site also revealed overestimation by WFDEI. Other differences which may be partly attributable to the urban setting of the observations include slightly warmer observed temperatures at night and lower observed relative humidity. The difference in elevation and measure-

Table A1
Details of WFDEI variables and conventions (Weedon et al., 2014) and the adjustments used to prepare 5-min input data for SUEWS. CRU precipitation totals were used.

Variable	WFDEI time period	WFDEI height	Adjustment
$K_{\downarrow}$	Average for previous 3 h	surface	Interpolated to 60 min
T_{air}	Instantaneous 3 h value	2 m	Interpolated to 60 min; unit conversion from K to °C
q, RH	Instantaneous 3 h value	2 m	Interpolated to 60 min; conversion from q [kg kg^{-1}] to RH [%]
P	Instantaneous 3 h value	10 m	Interpolated to 60 min
U	Instantaneous 3 h value	10 m	Interpolated to 60 min
P	Average rate for previous 3 h	surface	Distributed to 5-min; unit conversion from kg m^2 s^{-1} to mm

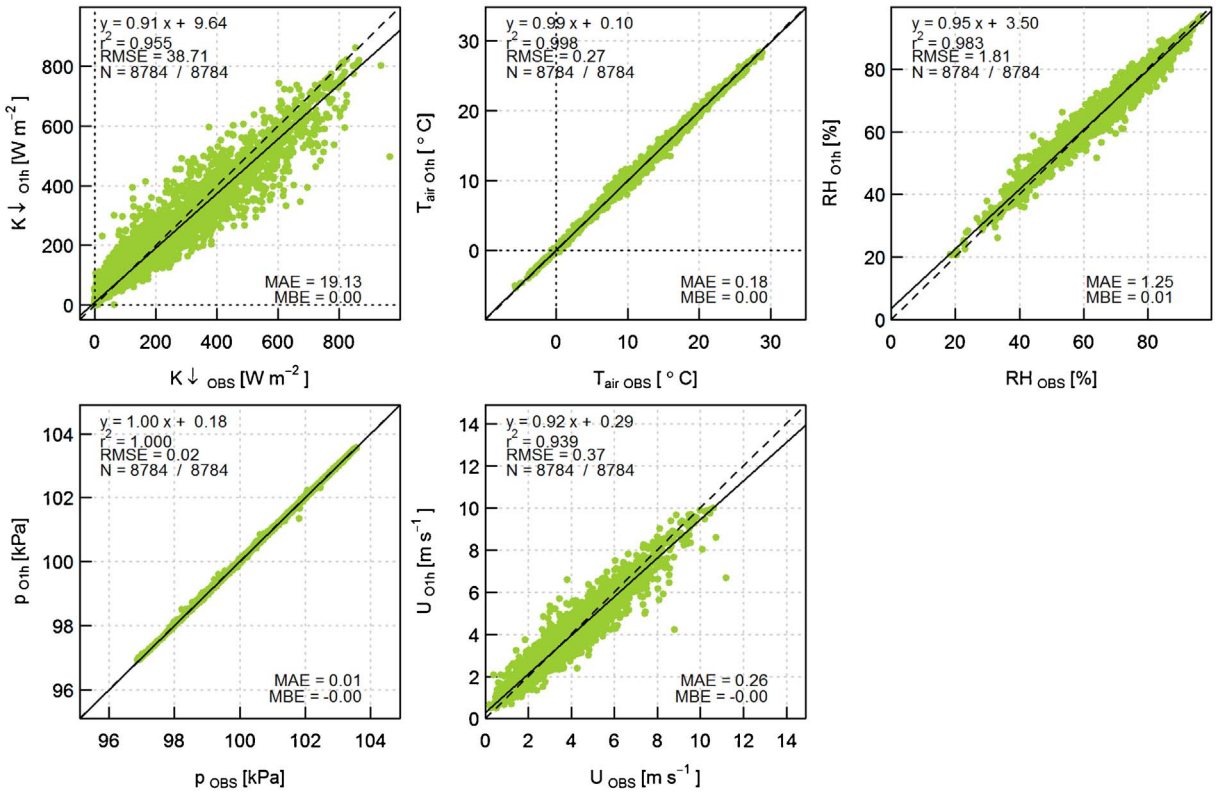

Fig. A1. Observed data averaged to 3 h then interpolated to 1 h ('O1h') versus observed data ('OBS') for the URB site in 2012. Statistics given are coefficient of determination (r^2), root mean square error (RMSE), number of hourly data points (N), mean absolute error (MAE) and mean bias error (MBE).

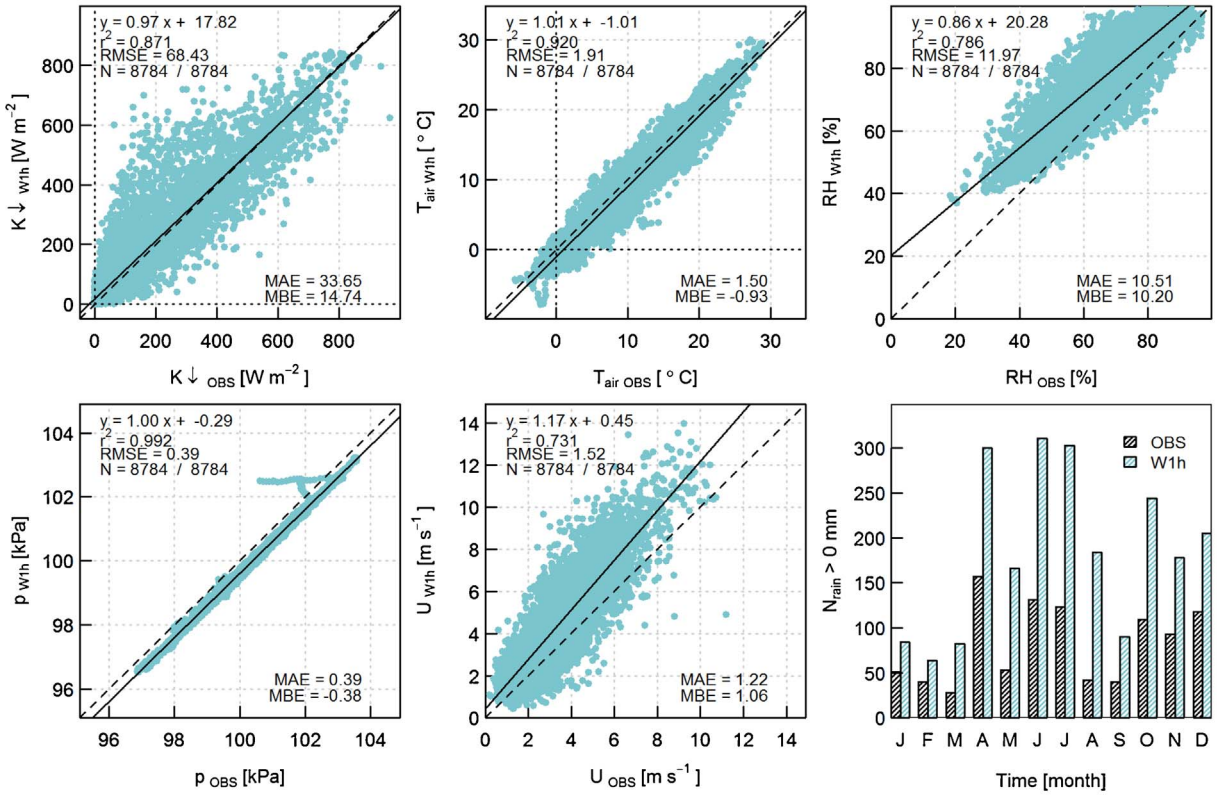

Fig. A2. As for Figure A1 but for 3-h WFDEI data interpolated to 1 h ('W1h') versus observed data ('OBS'). N_{rain} is the number of hourly data points with rain > 0 mm.

ment height contribute to small differences between the datasets, evident in the offset between p_{OBS} and p_{W1h}; the influence of height differences and urban roughness on wind speed is more complicated. However, the impact of these differences in T_{air}, p and U on the model output is very small and no attempt is made to adjust the WFDEI values. For locations in mountainous areas, it is advisable to check whether the elevation of the grid square is comparable to that of the study site, or if adjustments may be required Kokkonen et al., 2017).

A major difference occurs in the precipitation data, with the WFDEI dataset considerably wetter than OBS at both URB and SUB. In 2012, annual rainfall according to WFDEI (858 mm) is slightly larger than the observed total (821 mm at URB). According to OBS, rainfall occurs for 11% of the hourly periods; for the interpolated WFDEI dataset the value is 25%. The difference is also apparent in the original 3-h WFDEI dataset (18% compared to 29% of 3-h periods have rain). This increased frequency and volume of rainfall leads to an overestimation of modelled evaporation.

Out of the meteorological driving variables, SUEWS is most sensitive to P, $K_{\downarrow}$ and RH (as also found by Kokkonen et al. (2017)). For the sites and years considered here, using WFDEI data instead of observed forcing leads to an overestimation in Q^* and hence ΔQ_S, but the change in Q_H and Q_E is less significant because the effects of overestimated P and $K_{\downarrow}$ are partly compensated for by the overestimation of RH. For URB in 2012, using WFDEI data instead of observed forcing leads to an overestimation of about 20 W m^{-2} in Q^* compared to observations; the effect on Q_H and Q_E is smaller (< 7 W m^{-2} and < 5 W m^{-2} respectively).

Appendix B. Calculation of coefficients for anthropogenic heat flux model

Coefficients for the simple anthropogenic heat flux model (Eq. (2)) have been derived for several locations: North American cities (Sailor & Vasireddy, 2006), suburbs of Vancouver (Järvi et al., 2011), cold-climate cities of Helsinki and Montreal (Järvi et al., 2014), and at the URB and SUB sites Ward et al. (2016a). These coefficients differ, in part due to variation in building standards (i.e. insulation), energy use (e.g. air conditioning) and land use (residential, commercial, institutional). To calculate appropriate coefficients for use across London, the GreaterQF model (Iamarino et al., 2012) is used. As the most recent GreaterQF data are for 2008, the WFDEI air temperature for 2008 are used to calculate heating and cooling degree days, with a base human comfort temperature of 18.2 °C (Sailor & Vasireddy, 2006). Mean daily Q_F is compared with mean daily temperature, and the coefficients $a_{F0,1,2}$ fitted for each borough (Fig. B1). As the data suggest minimal use of air conditioning (i.e. little increase in Q_F at high temperatures), in accordance with expectations for the UK, a_{F1} is set to zero. The population density is taken as the mean of resident and workday values. Using resident/workday population densities alone gave much larger/smaller a_{F0} and a_{F2} values for inner boroughs, particularly those with contrasting day and night populations, whereas the mean gave a smaller range of a_{F0} and a_{F2} values and fewer extreme values.

Values of a_{F0} and a_{F2} are consistently higher for weekdays than weekends. a_{F0} ranged from 0.1134/0.1073 W m^{-2} (cap ha^{-1})$^{-1}$ on weekdays/weekends to 0.2281/0.2119 W m^{-2} (cap ha^{-1})$^{-1}$. a_{F2} ranged from 0.0038/0.0034 W m^{-2} K^{-1} (cap ha^{-1})$^{-1}$ on weekdays/weekends to 0.0076/0.0069 W m^{-2} K^{-1} (cap ha^{-1})$^{-1}$. In both cases, the lowest values are for Hackney and the highest for Hillingdon. No substantial difference is found between inner and outer boroughs, so the mean of the individual borough values is used for all model grids (Table B1). These values are slightly bigger than obtained for SUB and much smaller than for URB (Ward, Kotthaus et al., 2016), which is unsurprising given the characteristics of the observation sites relative to the boroughs. Note, Ward et al. (2016a) used Westminster borough population density (204.58 ha^{-1}) for URB. As the URB site is particularly densely built up, the borough average ρ_{pop} is likely an underestimation for this area which would explain the very large a_{F0} values obtained.

Building energy use is the greatest source of Q_F, contributing an average of 79% of the total, less in spring/summer more in autumn/winter (Fig. B2). Values range between 67% (Havering) and 92% (City of London). The vehicle contribution ranges from 6% (City of London) to 28% (Havering) with an average contribution of 15%. Human metabolism contributes between 2% (City of London) and 7% (Havering), with an average of 6%. Although building energy use varies substantially with temperature, the overall composition of Q_F is fairly constant throughout the year and Q_F is much lower in summer than winter.

For scenario 5, a 10% reduction in vehicle use is approximated by reducing a_{F0} by $0.10 \times 0.15 = 1.5\%$. A 20% reduction in building energy use is approximated by reducing a_{F0} and a_{F2} by $0.20 \times 0.79 = 15.8\%$. The resultant adjusted coefficients for scenario 5 are a_{F0} = 0.1346/0.1260 W m^{-2} (cap ha^{-1})$^{-1}$ and a_{F2} = 0.0045/0.0041 W m^{-2} K^{-1} (cap ha^{-1})$^{-1}$ for weekdays/weekends. For scenario 3, a_{F0} was reduced to 0.1457/0.1384 W m^{-2} (cap ha^{-1})$^{-1}$ for weekdays/weekends. These values were derived by fitting to GreaterQF data with the vehicle contribution halved. If instead, the approximation had been to reduce a_{F0} by $0.5 \times 15\% = 7.5\%$, slightly larger values of 0.1505 and 0.1409 W m^{-2} (cap ha^{-1})$^{-1}$ would have been obtained; this difference is mainly due to the variation in building energy use with temperature.

Appendix C. Estimating change in building density with population growth

Population growth for scenario 4 is based on GLA (2014) projections. To house this additional population, it is assumed that an increase in building density is required. For scenarios 4ii-iii additional buildings are constructed on available land (i.e. vegetated and bare soil surfaces). To estimate the change in the surface cover fraction of buildings required, data from the base run are used to derive a relation between the fraction of buildings and population density (Fig. C1). From this relation (fitted to the solid circles in Fig. C1), the change in modelled building fraction between the current and projected population is calculated and added to the current building fraction to give the new building fraction (empty circles).

The non-linear equation accounts for the changing relation between building fraction and population density: as population density increases buildings are taller and living space decreases. However, this is a simplistic approach. The relation should not be used for very low population densities (below 10.5 ha^{-1} it returns $f_{buildings} < 0$). The fit is based on the mean of day- and night-time populations, so includes workers and residents, and the fraction of all buildings, so includes residential, commercial, industrial and institutional buildings. Therefore, the estimated change in $f_{buildings}$ includes new homes, places of work and services in an approximate sense, but these are not explicitly accounted for (nor their varying composition between boroughs). Furthermore, only the change in building fraction has been estimated; no additional roads or gardens are considered.

Instead of building horizontally, scenario 4iv considers the case where land cover fractions are unchanged but the new buildings are constructed vertically (i.e. new floors added to existing building areas) so mean building height increases. To estimate the new mean building height, the current mean building height is multiplied by the ratio of

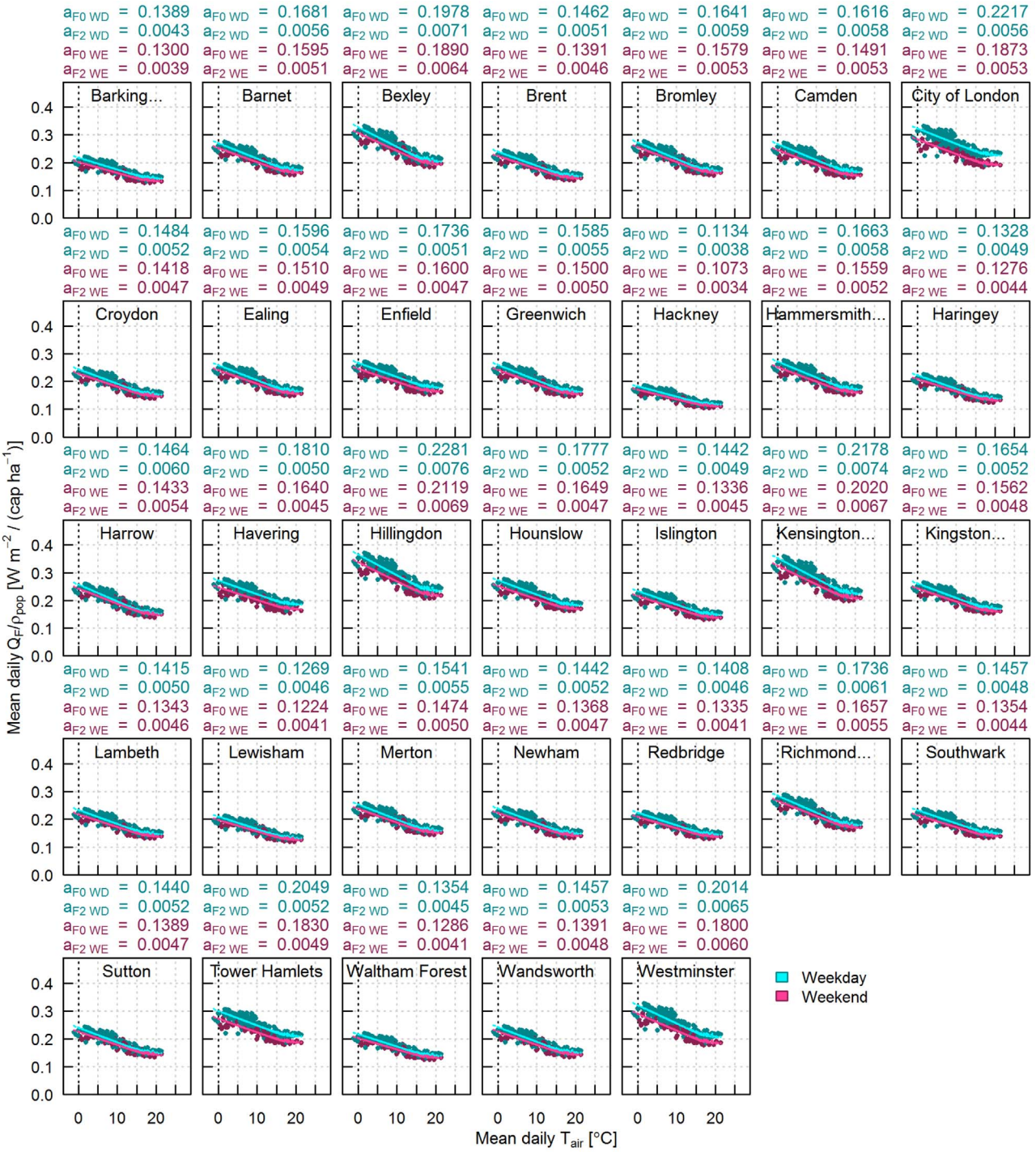

Fig. B1. Mean daily anthropogenic heat flux (normalised by population density) for each borough versus mean daily temperature for 2008. Fitted coefficients a_{F0} [W m^{-2} (cap ha^{-1})$^{-1}$] and a_{F2} [W m^{-2} K^{-1} (cap ha^{-1})$^{-1}$] are given separately for weekdays and weekends; a_{F1} was set to zero.

Table B1
Mean values of the coefficients derived for the London boroughs (LoBo). Values for URB and SUB are taken from Ward et al. (2016a) (note the night-time population of 47.63 ha^{-1} has been used to calculate the SUB values).

	LoBo Weekday	LoBo Weekend	URB Weekday	URB Weekend	SUB Weekday	SUB Weekend
a_{F0} [W m^{-2} (cap ha^{-1})$^{-1}$]	0.1627	0.1523	0.3743	0.3412	0.1446	0.1330
a_{F1} [W m^{-2} K^{-1} (cap ha^{-1})$^{-1}$]	0.0000	0.0000	0.0000	0.0000	0.0000	0.0000
a_{F2} [W m^{-2} K^{-1} (cap ha^{-1})$^{-1}$]	0.0054	0.0049	0.0073	0.0067	0.0037	0.0038

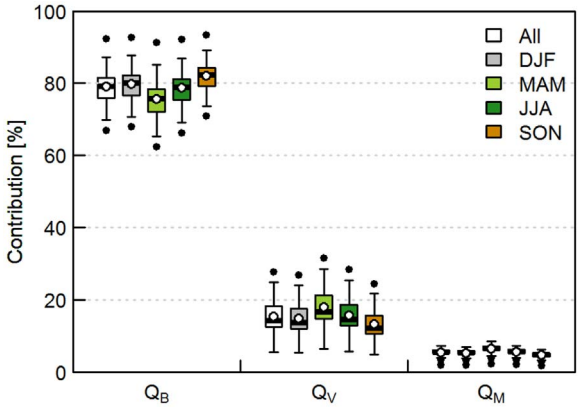

Fig. B2. Boxplots of the contribution of building energy use (Q_B), vehicle energy use (Q_V) and human metabolism (Q_M) to the total anthropogenic heat flux for each borough for the whole year and individual seasons. Mean values are plotted as empty circles; boxes enclose the inter-quartile range (IQR) with whiskers extending to the furthest point within 1.5 × IQR from the upper or lower quartile; in each case the outliers are Havering (lower outlier Q_B, upper outlier Q_V), City of London (upper outlier Q_B, lower outlier Q_M) and Westminster (lower outlier Q_M).

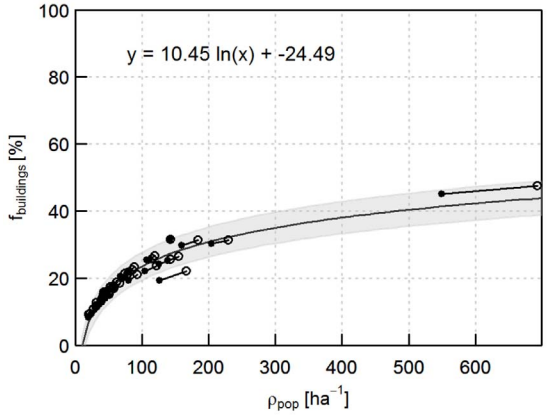

Fig. C1. Surface cover fraction of buildings as a function of population density for the base run (solid circles) and with 2020 projected population growth (empty circles) as for scenario 4. The equation of the line fitted to the solid circles is shown; shaded region indicates the standard error.

new to current $f_{buildings}$, giving the same change in building volume as before. In reality, of course, a mixture of horizontal and vertical development is likely.

References

Alexander, P. J., Mills, G., & Fealy, R. (2015). Using LCZ data to run an urban energy balance model. *Urban Climate*, *13*, 14–37.

Alexander, P. J., Fealy, R., & Mills, G. M. (2016). Simulating the impact of urban development pathways on the local climate: A scenario-based analysis in the greater Dublin region Ireland. *Landscape and Urban Planning*, *152*, 72–89.

Arnfield, A. J. (2003). Two decades of urban climate research: A review of turbulence, exchanges of energy and water, and the urban heat island. *International Journal of Climatology*, *23*(1), 1–26.

Beevers, S. D., & Carslaw, D. C. (2005). The impact of congestion charging on vehicle emissions in London. *Atmospheric Environment*, *39*(1), 1–5.

Bell, M. L., Goldberg, R., Hogrefe, C., Kinney, P. L., Knowlton, K., Lynn, B., et al. (2007). Climate change, ambient ozone, and health in 50 US cities. *Climatic Change*, *82*(1), 61–76.

Bergeron, O., & Strachan, I. B. (2010). Wintertime radiation and energy budget along an urbanization gradient in Montreal, Canada. *International Journal of Climatology*, *32*(1), 137–152.

Birkmann, J., & Welle, T. (2015). Assessing the risk of loss and damage: Exposure, vulnerability and risk to climate-related hazards for different country classifications. *International Journal of Global Warming*, *8*(2), 191–212.

Birkmann, J., Cutter, S. L., Rothman, D. S., Welle, T., Garschagen, M., van Ruijven, B., et al. (2015). Scenarios for vulnerability: Opportunities and constraints in the context of climate change and disaster risk. *Climatic Change*, *133*(1), 53–68.

Chen, J., Hill, A. A., & Urbano, L. D. (2009). A GIS-based model for urban flood inundation. *Journal of Hydrology*, *373*(1–2), 184–192.

Christen, A., & Vogt, R. (2004). Energy and radiation balance of a central European city. *International Journal of Climatology*, *24*(11), 1395–1421.

Dessai, S. (2002). Heat stress and mortality in Lisbon Part I. Model construction and validation. *International Journal of Biometeorology*, *47*(1), 6–12.

de Freitas, C. R., & Grigorieva, E. A. (2015). A comprehensive catalogue and classification of human thermal climate indices. *International Journal of Biometeorology*, *59*(1), 109–120.

de Munck, C., Pigeon, G., Masson, V., Meunier, F., Bousquet, P., Tréméac, B., et al. (2013). How much can air conditioning increase air temperatures for a city like Paris, France? *International Journal of Climatology*, *33*(1), 210–227.

Fischer, E. M., Seneviratne, S. I., Lüthi, D., & Schär, C. (2007). Contribution of land-atmosphere coupling to recent European summer heat waves. *Geophysical Research Letters*, *34*(6), L06707.

GLA (2005a). *Connecting Londoners with trees and Woodlands*. London: Greater London Authority.

GLA (2005b). *Crazy Paving: The environmental importance of London's front gardens*. London: Greater London Authority.

GLA (2011). *Branching out: The future for London's street trees*. London: Greater London Authority.

GLA (2012/3). GLA Median modelled household income 2012/13, http://data.london.gov.uk/dataset/household-income-estimates-small-areas.

GLA (2013). *London datastore: Daytime population*. Boroughhttp://data.london.gov.uk/dataset/daytime-population-borough.

GLA (2014). *GLA population projections 2014*. http://data.london.gov.uk/dataset/gla-population-projections-custom-age-tables.

Grimmond, C. S. B., & Oke, T. R. (1986). Urban water-balance 2 results from a suburb of Vancouver, British-Columbia. *Water Resources Research*, *22*(10), 1404–1412.

Grimmond, C. S. B., & Oke, T. R. (1991). An evapotranspiration-interception model for urban areas. *Water Resources Research*, *27*(7), 1739–1755.

Grimmond, C. S. B., & Oke, T. R. (1999a). Aerodynamic properties of urban areas derived from analysis of surface form. *Journal of Applied Meteorology*, *38*(9), 1262–1292.

Grimmond, C. S. B., & Oke, T. R. (1999b). Heat storage in urban areas: Local-scale observations and evaluation of a simple model. *Journal of Applied Meteorology and Climatology*, *38*, 922–940.

Grimmond, C. S. B., & Oke, T. R. (2002). Turbulent heat fluxes in urban areas: Observations and a local-scale urban meteorological parameterization scheme (LUMPS). *Journal of Applied Meteorology*, *41*(7), 792–810.

Grimmond, C. S. B., Oke, T. R., & Steyn, D. G. (1986). Urban water-balance 1 A model for daily totals. *Water Resources Research*, *22*(10), 1397–1403.

Grimmond, C. S. B., Cleugh, H. A., & Oke, T. R. (1991). An objective urban heat storage model and its comparison with other schemes. *Atmospheric Environment Part B. Urban Atmosphere*, *25*(3), 311–326.

Höppe, P. (1999). The physiological equivalent temperature – A universal index for the biometeorological assessment of the thermal environment. *International Journal of Biometeorology*, *43*(2), 71–75.

Hamilton, I. G., Davies, M., Steadman, P., Stone, A., Ridley, I., & Evans, S. (2009). The significance of the anthropogenic heat emissions of London's buildings: A comparison against captured shortwave solar radiation. *Building and Environment*, *44*(4), 807–817.

Howard, L. (1833). *The climate of London*. London: W. Phillips.

Hsieh, C., & Wu, K. (2012). Climate-sensitive urban design measures for improving the wind environment for pedestrians in a transit-oriented development area. *Journal of Sustainable Development*, *5*(4), 46.

IPCC (2012). *Special Report: Managing the risks of extreme events and disasters to advance climate change adaptation (SREX)*Cambridge University Press: Cambridge, UK.

Iamarino, M., Beevers, S., & Grimmond, C. S. B. (2012). High-resolution (space, time) anthropogenic heat emissions: London 1970–2025. *International Journal of Climatology*, *32*(11), 1754–1767.

Ichinose, T., Shimodozono, K., & Hanaki, K. (1999). Impact of anthropogenic heat on urban climate in Tokyo. *Atmospheric Environment*, *33*(24–25), 3897–3909.

Jáuregui, E., & Luyando, E. (1999). Global radiation attenuation by air pollution and its effects on the thermal climate in Mexico City. *International Journal of Climatology*, *19*(6), 683–694.

Järvi, L., Grimmond, C. S. B., & Christen, A. (2011). The surface urban energy and water balance scheme (SUEWS): Evaluation in los angeles and Vancouver. *Journal of Hydrology*, *411*(3–4), 219–237.

Järvi, L., Grimmond, C. S. B., Taka, M., Nordbo, A., Setälä, H., & Strachan, I. B. (2014). Development of the surface urban energy and water balance scheme (SUEWS) for cold climate cities. *Geosci. Model Dev*, *7*(4), 1691–1711.

Jarvis, P. G. (1976). The interpretation of the variations in leaf water potential and stomatal conductance found in canopies in the field. *Philosophical Transactions of the Royal Society of London B, Biological Sciences*, *273*(927), 593–610.

Jendritzky, G., de Dear, R., & Havenith, G. (2012). UTCI—Why another thermal index? *International Journal of Biometeorology*, *56*(3), 421–428.

Johansson, E., Thorsson, S., Emmanuel, R., & Krüger, E. (2014). Instruments and methods in outdoor thermal comfort studies – The need for standardization. *Urban Climate*, *10*(Part 2), 346–366.

Karsisto, P., Fortelius, C., Demuzere, M., Grimmond, C. S. B., Oleson, K. W., Kouznetsov, R., et al. (2015). Seasonal surface urban energy balance and wintertime stability simulated using three land-surface models in the high-latitude city Helsinki. *Quarterly Journal of the Royal Meteorological Society*, *142*(694), 401–417.

Klysik, K. (1996). Spatial and seasonal distribution of anthropogenic heat emissions in Łódź Poland. *Atmospheric Environment*, *30*(20), 3397–3404.

Kokkonen, T., Grimmond, C., Räty, O., Ward, H., Christen, A., Oke, T., Kotthaus, S., Järvi, L. (2017). Sensitivity of Surface Urban Energy and Water Balance Scheme (SUEWS) to downscaling of reanalysis forcing data.
Kotthaus, S., & Grimmond, C. S. B. (2014a). Energy exchange in a dense urban environment – Part II: Impact of spatial heterogeneity of the surface. *Urban Climate*, *10*, 281–307.
Kotthaus, S., & Grimmond, C. S. B. (2014b). Energy exchange in a dense urban environment – Part I: Temporal variability of long-term observations in central London. *Urban Climate*, *10*, 261–280.
Lee, H., Mayer, H., & Chen, L. (2016). Contribution of trees and grasslands to the mitigation of human heat stress in a residential district of Freiburg, Southwest Germany. *Landscape and Urban Planning*, *148*, 37–50.
Li, D., & Bou-Zeid, E. (2013). Synergistic interactions between urban heat islands and heat waves: The impact in cities is larger than the sum of its parts. *Journal of Applied Meteorology and Climatology*, *52*(9), 2051–2064.
Li, D., Sun, T., Liu, M., Yang, L., Wang, L., & Gao, Z. (2015). Contrasting responses of urban and rural surface energy budgets to heat waves explain synergies between urban heat islands and heat waves. *Environmental Research Letters*, *10*(5), 054009.
Lindberg, F., & Grimmond, C. S. B. (2011). Nature of vegetation and building morphology characteristics across a city: Influence on shadow patterns and mean radiant temperatures in London. *Urban Ecosystems*, *14*(4), 617–634.
Lindberg, F., Holmer, B., & Thorsson, S. (2008). SOLWEIG 1. 0–Modelling spatial variations of 3D radiant fluxes and mean radiant temperature in complex urban settings. *International Journal of Biometeorology*, *52*(7), 697–713.
Lindberg, F., Grimmond, C., Onomura, S., & Järvi, L. (2015). UMEP – An integrated tool for urban climatology and climate sensitive planning applications. *9th international conference on urban climate*.
Martins, T. A. L., Adolphe, L., Bonhomme, M., Bonneaud, F., Faraut, S., Ginestet, S., et al. (2016). Impact of Urban Cool Island measures on outdoor climate and pedestrian comfort: Simulations for a new district of Toulouse France. *Sustainable Cities and Society*, *26*, 9–26.
Masson, V., Marchadier, C., Adolphe, L., Aguejdad, R., Avner, P., Bonhomme, M., et al. (2014). Adapting cities to climate change: A systemic modelling approach. *Urban Climate*, *10*(Part 2), 407–429.
Mavrogianni, A., Davies, M., Batty, M., Belcher, S., Bohnenstengel, S., Carruthers, D., et al. (2011). The comfort, energy and health implications of London's urban heat island. *Building Services Engineering Research and Technology*, *32*(1), 35–52.
Met Office (2016). *Climate summaries*. http://www.metoffice.gov.uk/climate/uk/summaries.
Middel, A., Häb, K., Brazel, A. J., Martin, C. A., & Guhathakurta, S. (2014). Impact of urban form and design on mid-afternoon microclimate in Phoenix Local Climate Zones. *Landscape and Urban Planning*, *122*, 16–28.
Mills, G. (2007). Cities as agents of global change. *International Journal of Climatology*, *27*(14), 1849–1857.
Nakayama, T., & Fujita, T. (2010). Cooling effect of water-holding pavements made of new materials on water and heat budgets in urban areas. *Landscape and Urban Planning*, *96*(2), 57–67.
NeSS (2014). *Neighbourhood statistics*. www.neighbourhood.statistics.gov.uk/dissemination.
Ng, E., Chen, L., Wang, Y., & Yuan, C. (2012). A study on the cooling effects of greening in a high-density city: An experience from Hong Kong. *Building and Environment*, *47*, 256–271.
ONS (2011). *Office for national statistics – census 2011*. www.nomisweb.co.uk/census/2011.
Offerle, B., Grimmond, C. S. B., & Fortuniak, K. (2005). Heat storage and anthropogenic heat flux in relation to the energy balance of a central European city centre. *International Journal of Climatology*, *25*(10), 1405–1419.
Offerle, B., Grimmond, C. S. B., Fortuniak, K., & Pawlak, W. (2006). Intraurban differences of surface energy fluxes in a central European city. *Journal of Applied Meteorology and Climatology*, *45*(1), 125–136.
Ohashi, Y., Genchi, Y., Kondo, H., Kikegawa, Y., Yoshikado, H., & Hirano, Y. (2007). Influence of air-conditioning waste heat on air temperature in tokyo during summer: Numerical experiments using an urban canopy model coupled with a building energy model. *Journal of Applied Meteorology and Climatology*, *46*(1), 66–81.
Oke, T. R. (1982). The energetic basis of the urban heat-island. *Quarterly Journal of the Royal Meteorological Society*, *108*(455), 1–24.
Oke, T. R. (1987). *Boundary layer climates*. London, UK: Routledge, Taylor and Francis Group, 435.
Ramamurthy, P., Li, D., & Bou-Zeid, E. (2015). High-resolution simulation of heatwave events in New York City. *Theoretical and Applied Climatology*, 1–14.
Roberts, S. M., Oke, T. R., Grimmond, C. S. B., & Voogt, J. A. (2006). Comparison of four methods to estimate urban heat storage. *Journal of Applied Meteorology and Climatology*, *45*(12), 1766–1781.
Ryder, C. L., & Toumi, R. (2011). An urban solar flux island: Measurements from London. *Atmospheric Environment*, *45*(20), 3414–3423.
Sailor, D. J., & Fan, H. (2002). Modeling the diurnal variability of effective albedo for cities. *Atmospheric Environment*, *36*(4), 713–725.
Sailor, D. J., & Vasireddy, C. (2006). Correcting aggregate energy consumption data to account for variability in local weather. *Environmental Modelling & Software*, *21*(5), 733–738.
Sailor, D. J. (1995). Simulated urban climate response to modifications in surface albedo and vegetative cover. *Journal of Applied Meteorology*, *34*(7), 1694–1704.
Sailor, D. J. (2011). A review of methods for estimating anthropogenic heat and moisture emissions in the urban environment. *International Journal of Climatology*, *31*(2), 189–199.
Salmond, J. A., Tadaki, M., Vardoulakis, S., Arbuthnott, K., Coutts, A., Demuzere, M., et al. (2016). Health and climate related ecosystem services provided by street trees in the urban environment. *Environmental Health*, *15*(1), 95–111.
Schmid, H. P., Cleugh, H. A., Grimmond, C. S. B., & Oke, T. R. (1991). Spatial variability of energy fluxes in suburban terrain. *Boundary-Layer Meteorology*, *54*(3), 249–276.
Smith, C., Dawson, D., Archer, J., Davies, M., Frith, M., Hughes, E., et al. (2011). *From green to grey; observed changes in garden vegetation structure in London, 1998–2008*. London: London Wildlife Trust, Greenspace Information for Greater London, and Greater London Authority, London Wildlife Trust.
Song, T., & Wang, Y. (2012). Carbon dioxide fluxes from an urban area in Beijing. *Atmospheric Research*, *106*, 139–149.
Taha, H. (1997). Urban climates and heat islands: Albedo, evapotranspiration, and anthropogenic heat. *Energy and Buildings*, *25*(2), 99–103.
Theeuwes, N. E., Solcerová, A., & Steeneveld, G. J. (2013). Modeling the influence of open water surfaces on the summertime temperature and thermal comfort in the city. *Journal of Geophysical Research: Atmospheres*, *118*, 1–16.
Thorsson, S., Rocklöv, J., Konarska, J., Lindberg, F., Holmer, B., Dousset, B., et al. (2014). Mean radiant temperature – A predictor of heat related mortality. *Urban Climate*, *10*(Part 2), 332–345.
Tomlinson, C. J., Chapman, L., Thornes, J. E., & Baker, C. J. (2011). Including the urban heat island in spatial heat health risk assessment strategies: A case study for Birmingham, UK. *International Journal of Health Geographics*, *10*(1), 1–14.
Ward, H. C., Evans, J. G., & Grimmond, C. S. B. (2013). Multi-season eddy covariance observations of energy, water and carbon fluxes over a suburban area in Swindon, UK. *Atmospheric Chemistry and Physics*, *13*(9), 4645–4666.
Ward, H. C., Järvi, L., Onomura, S., Lindberg, F., & Grimmond, C. S. B. (2016a). *SUEWS manual: Version 2016*. http://urban-climate.net/umep/SUEWS.
Ward, H. C., Kotthaus, S., Järvi, L., & Grimmond, C. S. B. (2016b). Surface urban energy and water balance scheme (SUEWS): Development and evaluation at two UK sites. *Urban Climate*, *18*, 1–32.
Weedon, G. P., Gomes, S., Viterbo, P., Shuttleworth, W. J., Blyth, E., Österle, H., et al. (2011). Creation of the WATCH forcing data and its use to assess global and regional reference crop evaporation over land during the twentieth century. *Journal of Hydrometeorology*, *12*(5), 823–848.
Weedon, G. P., Balsamo, G., Bellouin, N., Gomes, S., Best, M. J., & Viterbo, P. (2014). The WFDEI meteorological forcing data set: WATCH Forcing Data methodology applied to ERA-Interim reanalysis data. *Water Resources Research*, *50*(9), 7505–7514.
Wolf, T., & McGregor, G. (2013). The development of a heat wave vulnerability index for London, United Kingdom. *W Eather and Climate Extremes*, *1*(0), 59–68.
Xiao, Q., McPherson, E. G., Simpson, J. R., & Ustin, S. L. (2007). Hydrologic processes at the urban residential scale. *Hydrological Processes*, *21*(16), 2174–2188.
Yu, H., Wang, P., Zong, X., Li, X., & Lü, D. (2010). Change of NO2 column density over Beijing from satellite measurement during the Beijing 2008 Olympic Games. *Chinese Science Bulletin*, *55*(3), 308–313.
Zhang, W., Lin Lawell, C. Y. C., & Umanskaya, V. I. (2017). The effects of license plate-based driving restrictions on air quality: Theory and empirical evidence. *Journal of Environmental Economics and Management*, *82*, 181–220.